Table 1 | Heart and body weight of EF;wt and EFCC mice

EF;wt			
Weeks	HW (mg)	BW (g)	HW (mg)/BW (g)
31	180	25.25	7.13
36	140	27.50	5.09
36	140	25.38	5.52
38	210	34.58	6.07
38	180	26.15	6.88
40	150	25.66	5.85
EFCC			
Weeks	HW (mg)	BW (g)	HW (mg)/BW (g)
30	360	19.63	18.34
35	640	25.47	25.12
36	320	25.66	12.47
36	260	22.49	11.56
40	410	23.66	17.33
42	120	16.22	7.40

not induce detectable translocations in such a rare cell type. Perhaps eSZ cell-specific *Cre* expression may enable the induction of Ewing's sarcoma by somatic *Ewsr1* and *Fli1* translocation, and efficient *Cre* expression in the specific spatiotemporal manner in the eSZ cell may be achieved using the promoter/enhancer elements of *Gdf5* or *Erg* genes[17,18].

Expression of *Ews-Fli1* in the majority of primary cells induced cellular apoptosis or senescence[19–21]. Activation of the *Casp3* promoter by EWS-FLI1 was reported, and the activation of caspase 3-dependent signals may be responsible for apoptotic processes in mouse embryonic fibroblasts (MEFs) with ectopic *Ews-Fli1* expression[21]. Indeed, *Ews-Fli1* expression in cardiac myocytes induced apoptotic cell death, though activation of caspase 3 was not detected in cardiac myocytes unlike in MEFs (data not shown). Thus, the low capacity for cardiac myocyte regeneration after birth could not support cardiac homeostasis. This limitation, therefore, could result in gradual but irreversible cardiac damage. In support of this idea, the *Ews-Fli1* fusion was not detected in the severely degenerated area but remained in relatively normal parts of the heart in EFCC mice. Moreover, introduction of *Ews-Fli1* cDNA significantly induced apoptosis in primary cardiac myocytes, indicating the cardiac toxicity of the fusion gene. The cell type-specific epigenetic status may modulate growth inhibitory and tumorigenic activities of EWS-FLI1. Indeed, different chromatin modification was observed between Ewing's sarcoma-sensitive eSZ and -resistant eGP cells[16]. It is noted that wild-type FLI1 protein represses *Col1a1* expression, inhibiting cardiac fibrosis[22]. Interestingly, EWS-FLI1 enhanced *COL1A1* expression in human cardiac fibroblasts, suggesting that it might accelerate fibrotic processes in cardiomyopathy.

A number of transcription factors are associated with the development and maintenance of cardiac myocytes, and mutations in these factors affect cardiac homeostasis, structure and functions[23]. Over-expression of *E2F6* activates gene expression in myocardium and induces dilated cardiomyopathy in mice[24]. Moreover, mutations in *NKX2-5* and *PDRM16* were found associated with human congenital dilated cardiomyopathy[25,26]. It has been proposed that these proteins regulate genes involved in the ubiquitin proteasome system or proliferation of cardiomyocytes, suggesting different aspects of myocardial damage from the present model. Nevertheless, similar phenotypes shown in these models indicate the importance of cardiac-specific transcriptional regulation by transcription factors, given the low regenerative activity of adult cardiomyocytes.

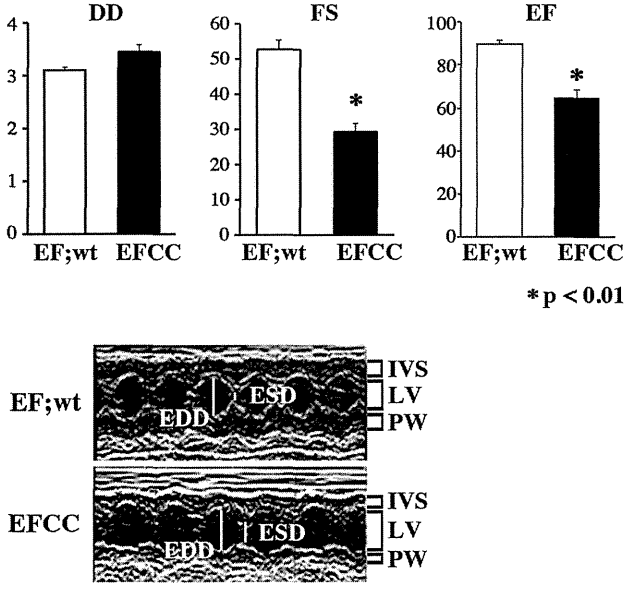

Figure 5 | Echocardiographic analysis of 37-week-old EFCC and EF;wild-type mice. Analysis of cardiovascular function (top). DD, diastolic diameter of left ventricle; FS, fractional shortening; EF, ejection fraction. Representative echocardiogram for wild-type and EFCC mice (bottom). EDD, end-diastolic diameter; ESD, end-systolic diameter, IVS, interventricular septum; LV, left ventricle; PW, posterior wall.

Methods

Mice and gene targeting. The *Ewsr1* and *Fli1* targeting vectors were assembled in a pBSKSTKLoxPNeoGFP plasmid containing appropriate *lox*P sites, a *lox*P-flanked thymidine kinase (*Tk*) promoter-driven *neo* gene and a *Tk* promoter-driven diphtheria toxin gene. A *Gfp* gene was inserted immediately downstream of the 3′ *lox*P site for the *Ewsr1* vector. The homologous regions of the *Ewsr1* vector consisted of an 8.4 kb genomic fragment containing *Ewsr1* exons 5 to 7 and a 1.3 kb flanking exon 8 (Fig. 1a). Similarly, the *Fli1* vector included a 5.4 kb genomic fragment of *Fli1* intron 5 and a 2.0 kb fragment flanking exon 6. A CMV promoter sequence was also inserted immediately upstream of the 5′ *lox*P site of the *Fli1* vector. To establish mice carrying a single *lox*P allele of *Ewsr1* or *Fli1* genes, the linearized targeting vectors were electroporated into E14 ES cells, and drug-resistant colonies were screened for homologous recombination. To remove the *lox*P-flanked neomycin-resistant gene cassette, the pMCCreGKPuro vector was electroporated into the ES cells, and puromycin-resistant colonies were selected. Targeted clones were injected into C57BL/6 blastocysts and the resultant chimeric mice were bred to produce progeny having germ line transmission of the mutated allele. Mice harboring a targeted *Ewsr1* allele ($Ewsr1^{lx/+}$) and a targeted *Fli1* allele ($Fli1^{lx/+}$) were crossed to establish the mice that possessed *lox*P sites both in *Ewsr1* intron 7 and in *Fli1* intron 5. The resultant

Table 2 | Echocardiographic and hemodynamic analysis

	E/F; wt (n=3)	EFCC (n=4)
Echocardiographic data		
LVDd (mm)	3.01 ± 0.06	3.45 ± 0.13
LVDs (mm)	1.43 ± 0.07	2.43 ± 0.14
IVST (mm)	1.07 ± 0.03	0.78 ± 0.08
LVPWT (MM) **	1.06 ± 0.01	0.76 ± 0.04
FS (%)*	52.67 ± 2.67	29.25 ± 2.43
EF (%)*	89.67 ± 1.67	64.75 ± 3.75
Hemodynamic data		
HR (bpm)	580.7 ± 36.7	631.5 ± 11.9
sBP (mm Hg)	104.3 ± 3.8	105.5 ± 1.4
dBP (mm Hg)	57.7 ± 7.4	50.8 ± 4.5

Values are means ± SEM. LVDd, left ventricular end-diastolic dimension; LVDs, LV end-systolic dimension; IVST, interventricular septum thickness; LVPWT, left ventricular posterior wall thickness; FS, fractional shorting; EF, ejection fraction; HR, heart rate; sBP, systolic blood pressure; dBP, diastolic blood pressure; *, $p < 0.01$; **, $p < 0.05$.

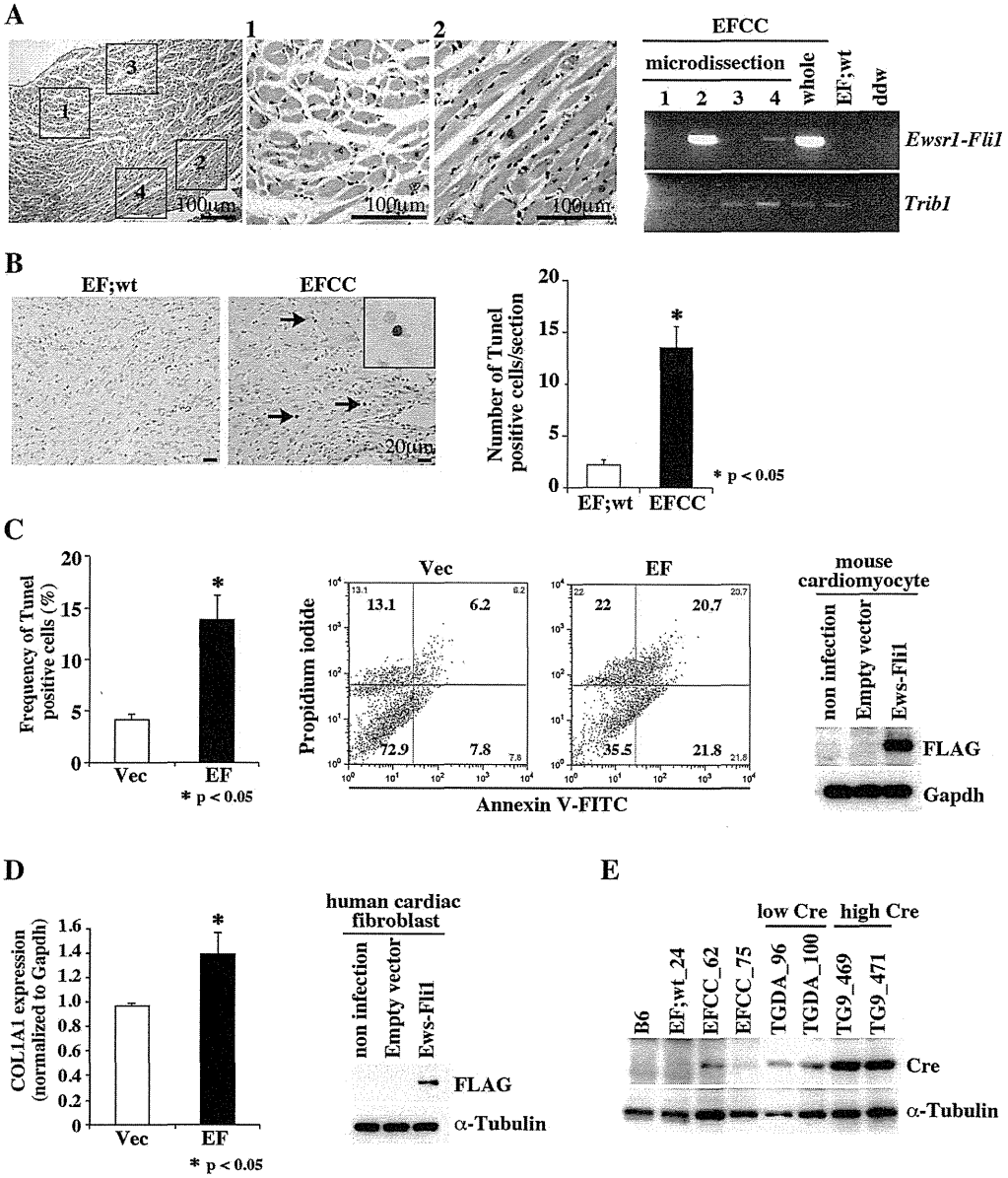

Figure 6 | The cardiac lesion in the EFCC mouse and *Ewsr1-Fli1* translocation. (A) Detection of *Ewsr1-Fli1* translocation in the myocardium. The frozen section of the cardiac tissue from the EFCC mouse was laser microdissected for the indicated areas (1-4) (left). Genomic PCR using DNA samples obtained by laser microdissection (right). (B) A TUNEL assay showed a significantly greater increase of apoptotic cell death in the myocardium of the EFCC mouse than in that of the wild-type mouse (left). High power view of the apoptotic cell is shown in the magnified inset. Frequencies of TUNEL-positive cells per section are compared between wild type and EFCC mice (right). (C) *Ewsr1-Fli1* cDNA expression induced apoptotic cell death of cardiac myocytes *in vitro*. The apoptotic cells were measured by positive signals in a TUNEL assay (left). Ewsr1-Fli1-induced cell death was further analyzed by Annexin V/PI staining and FACS analysis. The lower right quadrant (Annexin V+/PI-) represents early apoptosis, while the upper right quadrant (Annexin V+/PI+) and the upper left quadrant (Annexin V-/PI+) represent late apoptosis and necrosis, respectively. Data are representatives of three independent experiments with similar results (center). The expression of EWS-FLI1 protein in cardiac myocytes was detected by Western blotting using anti-FLAG M2 antibody (right). (D) Quantitative real-time RT-PCR for COL1A1 in human cardiac fibroblasts with or without Ewsr1-Fli1 (left). Expression of EWS-FLI1 protein was detected by Western blotting using anti-FLAG M2 antibody (right). (E) Expression of the Cre protein in the heart of EFCC mice and other *Cre* transgenic lines of variable expression levels[12].

Ewsr1$^{fl/+}$ and *Fli1*$^{fl/+}$ mice were further crossed with *CAG-Cre*, *Mx1-Cre* or *Rosa26-CreER* mice[27–29]. Genotyping of the mice was performed using primers described below. Animals were handled in accordance with the guidelines of the animal care committee at the Japanese Foundation for Cancer Research, which gave ethical approval for these studies.

Southern blotting. Southern blotting was carried out using standard procedures[30]. Genomic DNA samples were digested with *Xba*I or *Sac*I and probed with genomic DNA fragments derived from *Ewsr1* or *Fli1* loci (Fig. 1a).

Fluorescence *in situ* hybridization (FISH). The BAC clones, RPCI-23 64E17 downstream from *Ewsr1* on mouse chromosome 11 and RPCI-23 218O31 upstream from *Fli1* on chromosome 9 were purchased from Invitrogen (Carlsbad, CA) for FISH analysis. The FISH analysis using metaphase spreads obtained from embryonic fibroblasts of the *Ewsr1*$^{fl/+}$:*Fli1*$^{fl/+}$:*CAG-Cre* (EFCC) mouse was performed according to the methods previously described[31].

Genomic and reverse transcription-polymerase chain reaction (gPCR and RT-PCR). Genomic DNA (100 ng) was subjected to 35 cycles of PCR amplification. The

PCR primers to detect the *Ewsr1-Fli1* fusions were as follows. For *Ewsr1-Fli1, Ewsr1* forward primer 5′-ccccagtgcttatccttacatttg-3′ and *Fli1* reverse primer 5′-cctgacccgtgtctttgtag-3′, and for *Fli1-Ewsr1, Fli1* forward primer 5′-agagaacccactgcttactgg-3′ and Ewsr1 reverse primer 5′-accacgccctccaggttcac-3′ were used. To detect the rare translocation in *Rosa26-CreER* and *Mx1-Cre* transgenic mice, genomic DNA samples were pre-amplified using 35 cycles of PCR using the following primers. For *Ewsr1,* the 5′ primer was 5′-ccaagtaggggctctgtcag-3′ and for *Fli1,* the 3′ primer was 5′-ggagctgaagcagtaggaag-3′. For *Fli1,* the 5′ primer was 5′-gccccattgacgcaaatggg-3′ and for Ewsr1, the 3′ primer was 5′-ggggtacttggtgaaggtgc-3′. Genomic PCR for the wild-type *Ewsr1* transgene, Cre recombinase or *Trib1* was performed using the following primers: *Ewsr1,* forward, 5′-cccagtgcttatccttacatttg-3′ and GFP, reverse, 5′-accacgccctccaggttcac-3′, Cre, forward, 5′-catacctggaaaatgcttctgtcc-3′ and Cre, reverse, 5′-attgctgtcacttggtcgtggc-3′, or *Trib1,* forward, 5′-cagtctctccttccaagtcatc-3′ and *Trib1,* reverse, 5′-gattgttgctgctgttgttc-3′. The PCR products were analyzed by 2% agarose gel electrophoresis.

RT-PCR was carried out using cDNA generated from total RNA of systemic organs as previously described[32]. The *Ewsr1-Fli1* fusion transcript was amplified using *Ewsr1* exon 7 primer (5′-tcctcttcacagccgac-3′) and *Fli1* exon 6 primer (5′-ctgctcagtgttcttgcc-3′). The primers for Cre recombinase (forward, 5′-cggtctggcagtaaaaactat-3′; reverse, 5′-cagggtgttataagcaatccc-3′) and *Hprt* (forward, 5′-gctggtgaaaaggacctct-3′; reverse, 5′-cacaggactagaacacctgc-3′) were also used. The PCR products were purified, subcloned into a plasmid and sequenced. Real-time quantitative RT-PCR was performed by using a Fast Real-Time PCR System (Applied Biosystems, Foster City, CA). The primers for human *COL1A1* (forward, 5′-catgaccgagacgtgtggaa-3′; reverse, 5′-tttcttggtcggtgggtgac-3′) and GAPDH (forward, 5′-acctgacctgccgtctagaa-3′; reverse, 5′-aaagtggtcgttgagggcaa-3′) were used.

Echocardiography. Transthoracic echocardiography was performed on conscious, gently restrained mice using a 15-MHz linear probe (Power-Vision 8000, Toshiba, Tokyo, Japan), as described previously[33]. Parasternal long-axis view and short axis view of the left ventricle at the level of the papillary muscles were obtained. 2D-guided M-mode recordings were obtained from short axis view at the level of the papillary muscles. Measurements of interventricular septum thickness (IVST) and left ventricular posterior wall thickness (LVPWT) were made from M-mode recordings in diastole. Left ventricular internal diameter at end-diastole (LVDd) and end-systole (LVDs) were measured from M-mode recordings. Fractional shortening (FS) was calculated as $100 \times [(\mathrm{LVDd} - \mathrm{LVDs})/\mathrm{LVDd}]$ (%). Ejection fraction (EF) was calculated using the Teichholtz method.

Cell culture and recombinant lentivirus infection. Primary neonatal ICR mouse ventricular myocytes were purchased from Cosmo Bio (Tokyo, Japan), and cells were cultured with D-MEM/F-12 medium supplemented 10% fetal bovine serum (HyClone, South Logan, UT). Human cardiac fibroblasts were purchased from PromoCell (Heidelberg, Germany), and cells were cultured with Fibroblast Medium (ScienCell, Carlsbad, CA). The human *EWSR1-FLI1* cDNA (a kind gift from Susanne Baker) was FLAG-tagged and inserted into the pLVSIN-CMV-neo plasmid (Takara Bio, Tokyo, Japan) and HEK 293 cells were transfected with the plasmid using Lipofectamine 2000 (Invitrogen). Cells were harvested 48 h after lentiviral infection and subjected to further analyses.

TUNEL assay and Annexin-V analysis. Formaldehyde-fixed and paraffin-embedded cardiac tissue sections or methanol-fixed murine primary cardiac myocytes were subjected to TUNEL assays using the DeadEnd Colorimetric TUNEL System (Promega, Madison, WI) according to the manufacturer's protocol. For the Annexin V analysis cells were stained with Annexin V-FITC and propidium iodide (PI) according to the manufacturer's instruction (BD Bioscience Pharmingen, San Diego, CA). The stained cells were immediately evaluated using a FACSCalibur flow cytometer (BD Biosciences, Franklin Lakes, NJ).

Western blotting. Western blotting was performed as previously described[32]. A monoclonal anti-FLAG M2 antibody was purchased from Sigma (St Louis, MO), anti-Cre from Chemicon (Temecula, CA), anti-α-tubulin from Sigma and anti-GAPDH from HyTest (Turku, Finland).

Statistical analysis. Results are shown as means ± standard errors of the mean (SEM). Continuous distributions were compared with two-tailed Student's *t*-tests. Survival analysis was performed using the Kaplan-Meier life table method, and the survival between groups was compared with the log-rank test. All *P* values were two-sided, and a *P* value of less than 0.05 was considered significant.

1. Mitelman, F., Johansson, B. & Mertens, F. The impact of translocation and gene fusions on cancer causation. *Nat. Rev. Cancer* **7**, 233–245 (2007).
2. Taylor, B. S. *et al.* Advances in sarcoma genomics and new therapeutic targets. *Nat. Rev. Cancer* **11**, 541–557 (2011).
3. Smith, A. J. H. *et al.* A site-directed chromosomal translocation induced in embryonic stem cells by Cre-*lox*P recombination. *Nat. Genet.* **9**, 376–385 (1995).
4. Van Deursen, J., Fornerod, M., van Rees, B. & Grosveld, G. Cre-mediated site-specific translocation between nonhomologous mouse chromosomes. *Proc. Natl. Acad. Sci. USA* **92**, 7376–7380 (1995).
5. Forster, A. *et al.* Engineering de novo reciprocal chromosomal translocations associated with *Mll* to replicate primary events of human cancer. *Cancer Cell* **3**, 449–458 (2003).
6. Delattre, O. *et al.* Gene fusion with an *ETS* DNA-binding domain caused by chromosome translocation in human tumours. *Nature* **359**, 162–165 (1992).
7. Sorensen, P. H. *et al.* A second Ewing's sarcoma translocation, t(21;22), fuses the EWS gene to another ETS-family transcription factor, ERG. *Nat. Genet.* **6**, 146–151 (1994).
8. Ordonez, J. L., Osuna, D., Herrero, D., de Alava, E. & Madoz-Gurpide, J. Advances in Ewing's sarcoma research: where are we now and what lies ahead? *Cancer Res.* **69**, 7140–7150 (2009).
9. Torchia, E. C., Boyd, K., Rehg, J. E., Qu, C. & Baker, S. J. *EWS/FLI-1* induces rapid onset of myeloid/erythroid leukemia in mice. *Mol. Cell. Biol.* **27**, 7918–7934 (2007).
10. Zucman, J. *et al.* Combinatorial generation of variable fusion proteins in the Ewing family of tumours. *EMBO J.* **12**, 4481–4487 (1993).
11. Riggi, N., Cironi, L., Suva, M. L. & Stamenkovic, I. Sarcomas: genetics, signaling, and cellular origins. Part I: The fellowship of TET. *J. Pathol.* **213**, 4–20 (2007).
12. Buerger, A. *et al.* Dilated cardiomyopathy resulting from high-level myocardial expression of Cre-recombinase. *J. Card. Fail.* **12**, 392–398 (2006).
13. Collins, E. C., Pannell, R., Simpson, E. M., Forster, A. & Rabbitts, T. H. Inter-chromosomal recombination of *Mll* and *Af9* genes mediated by cre-*loxP* in mouse development. *EMBO Rep.* **1**, 127–132 (2000).
14. Drynan, L. F. *et al. Mll* fusions generated by Cre-*loxP*-mediated *de novo* translocations can induce lineage reasignment in tumorigenesis. *EMBO J.* **24**, 3136–3146 (2005).
15. Buchholz, F., Regaeli, Y., Trumpp, A. & Bishop, J. M. Inducible chromosomal translocation of *AML1* and *ETO* genes through Cre/loxP-mediated recombination in the mouse. *EMBO Rep.* **11**, 133–139 (2000).
16. Tanaka, M. *et al.* Ewing's sarcoma precursors are highly enriched in embryonic osteochondrogenic progenitors. *J. Clin. Invest.* **121**, 3061–3074 (2014).
17. Storm, E. E. & Kingsley, D. M. GDF5 coordinates bone and joint formation during digit development. *Dev. Biol.* **209**, 11–27 (1999).
18. Vijayaraj, P. *et al.* Erg is a crucial regulator of endocardial-mesenchymal transformation during cardiac valve morphogenesis. *Development* **139**, 3973–3985 (2012).
19. Deneen, B. & Denny, C. T. Loss of p16 pathways stabilizes EWS/FLI1 expression and complements EWS/FLI1 mediated transformation. *Oncogene* **20**, 6731–6741 (2001).
20. Lessnick, S. L., Dacwag, C. S. & Golub, T. R. The Ewing's sarcoma oncoprotein EWS/FLI induces a p53-dependent growth arrest in primary human fibroblasts. *Cancer Cell* **1**, 393–401 (2002).
21. Sohn, E. J. *et al.* EWS/FLI1 oncogene activates caspase 3 transcription and triggers apoptosis *in vivo*. *Cancer Res.* **70**, 1154–1163 (2010).
22. Elkareh, J. *et al.* Marinobufagenin induces increases in procollagen expression in a process involving protein kinase C and Fli-1: implications for uremic cardiomyopathy. *Am. J. Physiol. Renal. Physiol.* **296**, F1219–F1226 (2009).
23. Oka, T., Xu, J. & Molkentin, J. D. Re-employment of developmental transcription factors in adult heart disease. *Semin. Cell Dev. Biol.* **18**, 117–131 (2007).
24. Westendorp, B. *et al.* The E2F6 repressor activates gene expression in myocardium resulting in dilated cardiomyopathy. *FASEB J.* **26**, 2569–2579 (2012).
25. Costa, M. W. *et al.* Functional characterization of a novel mutation in *NKX2-5* associated with congenital heart disease and adult-onset cardiomyopathy. *Circ. Cardiovasc. Genet.* **6**, 238–247 (2013).
26. Arndt, A. K. *et al.* Fine mapping of the 1p36 deletion syndrome identifies mutation of *PRDM16* as a cause of cardiomyopathy. *Am. J. Hum. Genet.* **93**, 67–77 (2013).
27. Sakai, K. & Miyasaki, J. A transgenic mouse line that retains Cre recombinase activity in mature oocytes irrespective of the cre transgene transmission. *Biochem. Biophys. Res. Commun.* **237**, 318–324 (1997).
28. Kuhn, R., Schwenk, F., Aguet, M. & Rajewsky, K. Inducible gene targeting in mice. *Science* **269**, 1427–1429 (1995).
29. Ventura, A. *et al.* Restoration of p53 function leads to tumour regression *in vivo*. *Nature* **445**, 661–665 (2007).
30. Iwasaki, M. *et al.* Identification of cooperative genes for NUP98-HOXA9 in myeloid leukemogenesis using a mouse model. *Blood* **105**, 784–793 (2005).
31. Kawamura-Saito, M. *et al.* Fusion between CIC and DUX4 up-regulates PEA3 family genes in Ewing-like sarcomas with t(4;19)(q35;q13) translocation. *Hum. Mol. Genet.* **15**, 2125–2137 (2006).
32. Nakamura, T. *et al.* Evi9 encodes a novel zinc finger protein that interacts with BCL6, a known human B-cell proto-oncogene. *Mol. Cell. Biol.* **20**, 3178–3186 (2009).
33. Kuwahara, K. *et al.* NRSF regulates the fetal cardiac gene program and maintains normal cardiac structure and function. *EMBO J.* **22**, 6310–6321 (2003).

Acknowledgments

We are grateful to Junichi Miyazaki for CAG-Cre, Klaus Rajewsky for MX1-Cre and Tyler Jacks for Rosa26-Cre transgenic mice. We also thank Miki Yamazaki, Yohei Kanno, Hitomi Yamanaka and Tokuichi Kawaguchi for technical assistance. This work was supported by

the Grants-in-Aid for Scientific Research from the Ministry of Education, Culture, Sports, Science and Technology (23791672 and 26250029) to M.T. and T.Na.

Author contributions

M.T., T.No. and T.Na. designed the work. M.T., S.Y., Y.Y. and H.K. performed the experiments. M.T., K.K., K.N., P.Y.J., T.No. and T.Na. analyzed the data. M.T. and T.Na. wrote the paper. All co-authors contributed in the form of discussion and critical comments.

Additional information

Competing financial interests: The authors declare no competing financial interests.

How to cite this article: Tanaka, M. *et al.* Somatic chromosomal translocation between *Ewsr1* and *Fli1* loci leads to dilated cardiomyopathy in a mouse model. *Sci. Rep.* **5**, 7826; DOI:10.1038/srep07826 (2015).

Journal of Molecular and Cellular Cardiology 80 (2015) 81–89

Contents lists available at ScienceDirect

Journal of Molecular and Cellular Cardiology

journal homepage: www.elsevier.com/locate/yjmcc

Original article

Ectopic automaticity induced in ventricular myocytes by transgenic overexpression of HCN2

Kensuke Oshita [a,b], Masayuki Itoh [a], Shingo Hirashima [c], Yoshihiro Kuwabara [d], Keiko Ishihara [a], Koichiro Kuwahara [d], Kazuwa Nakao [e,f], Takeshi Kimura [d], Kei-ichiro Nakamura [c], Kazuo Ushijima [b], Makoto Takano [a,*]

[a] Department of Physiology, Kurume University School of Medicine, Kurume, Japan
[b] Department of Anesthesiology, Kurume University School of Medicine, Kurume, Japan
[c] Division of Microscopic and Developmental Anatomy, Department of Anatomy, Kurume University School of Medicine, Kurume, Japan
[d] Department of Cardiovascular Medicine, Graduate School of Medicine, Kyoto University, Kyoto, Japan
[e] Medical Innovation Center, Graduate School of Medicine, Kyoto University, Kyoto, Japan
[f] Department of Medicine and Clinical Science, Graduate School of Medicine, Kyoto University, Kyoto, Japan

ARTICLE INFO

Article history:
Received 16 July 2014
Received in revised form 5 December 2014
Accepted 22 December 2014
Available online 3 January 2015

Keywords:
HCN2
Arrhythmia
Ion channel
Cardiomyocyte
Electrophysiology

ABSTRACT

Hyperpolarization-activated cyclic nucleotide-gated channels (HCNs) are expressed in the ventricles of fetal hearts but are normally down-regulated as development progresses. In the hypertrophied heart, however, these channels are re-expressed and generate a hyperpolarization-activated, nonselective cation current (I_h), which evidence suggests may increase susceptibility to arrhythmia. To test this hypothesis, we generated and analyzed transgenic mice overexpressing HCN2 specifically in their hearts (HCN2-Tg). Under physiological conditions, HCN2-Tg mice exhibited no discernible abnormalities. After the application of isoproterenol (ISO), however, ECG recordings from HCN2-Tg mice showed intermittent atrioventricular dissociation followed by idioventricular rhythm. Consistent with this observation, 0.3 μmol/L ISO-induced spontaneous action potentials (SAPs) in 76% of HCN2-Tg ventricular myocytes. In the remaining 24%, ISO significantly depolarized the resting membrane potential (RMP), and the late repolarization phase of evoked action potentials (APs) was significantly longer than in WT myocytes. Analysis of membrane currents revealed that these differences are attributable to the I_h tail current. These findings suggest HCN2 channel activity reduces the repolarization reserve of the ventricular action potential and increases ectopic automaticity under pathological conditions such as excessive β-adrenergic stimulation.

1. Introduction

Hyperpolarization-activated cyclic nucleotide-gated channels (HCNs) are widely expressed in a variety of tissues [1]. Among the four HCN subtypes (HCN1-4), HCN2 and HCN4 are abundantly expressed in the pacemaker cells of the sinoatrial node, where they generate a hyperpolarization-activated, nonselective cation current (I_f/I_h), which plays a key role in cardiac pacemaker activity [2]. HCN2 and 4 are also expressed in ventricular myocytes early during fetal development but are down-regulated at later stages [3,4].

As many as 50% of patients with heart failure die from sudden cardiac death, most likely caused by a lethal arrhythmia [5]. In heart failure and cardiac hypertrophy, the cardiac remodeling process reactivates ventricular myocardial expression of such fetal cardiac genes as HCN2 and HCN4 as well as CACNA1G and CACNA1H, which encode T-type Ca^{2+} channel subunits [6–8]. Although the mechanisms responsible for lethal arrhythmias in failing hearts remain unresolved, evidence suggests re-expression of fetal type cardiac ion channels contributes to the arrhythmogenicity. Indeed, when we generated transgenic mice that selectively expressed a dominant-negative neuron-restrictive silencer factor mutant in their hearts (dnNRSF-Tg mice), we found that these mice experienced sudden arrhythmic death and that there was a concomitant up-regulation of fetal type cardiac ion channels [9]. However, the contribution of each fetal cardiac channel to the arrhythmogenicity remains uncertain.

We previously reported that pharmacological blockade of HCN channels partially suppressed sudden arrhythmic death in dnNRSF-Tg mice [9]. We also carried out a preliminary analysis of transgenic mice overexpressing HCN2 in their hearts (HCN2-Tg) and reported that they were vulnerable to β-adrenergic-induced abnormal electrical activity [10]. In the present study, we carried out a detailed analysis of

* Corresponding author at: Department of Physiology, Kurume University School of Medicine, 67 Asahi-machi, Kurume 830-0011, Japan. Tel.: +81 942 31 7543; fax: +81 942 31 7728.
E-mail address: takanom@med.kurume-u.ac.jp (M. Takano).

http://dx.doi.org/10.1016/j.yjmcc.2014.12.019

the electrocardiographic and electrophysiological properties of single ventricular myocytes from HCN2-Tg mice. Our findings demonstrate that HCN2 channel activity reduces the repolarization reserve of the ventricular action potential (AP) and increases the ectopic automaticity of ventricular myocytes.

Preliminary results from this study were communicated at the annual meeting of the Japanese Physiological Society (Tokyo 2013) and at the Congress of the International Union of the Physiological Society (Birmingham 2013) [11].

2. Materials and methods

All animal experiments were approved in advance by the Animal Ethics Committee of Kurume University (No. 23-11). Animal care and experiments conform to the Guidelines for the Care and Use of Laboratory Animals published by the US National Institutes of Health (NIH Publication No. 85-23, revised 1996).

2.1. Experimental animals

We overexpressed mouse HCN2 cDNA in the hearts of C57BL/6 mice using the α-MHC promoter (HCN2-Tg) [10]. HCN2-Tg and their wild-type (WT) littermates were used while they were between 10 and 14 weeks of age.

2.2. Cell isolation

After deeply anesthetizing mice using 3.0% sevoflurane, their hearts were quickly removed and the ventricular myocytes were isolated through collagenase digestion [12].

2.3. Heterologous expression experiment

Mouse HCN2 cDNA was subcloned into pCDNA3 vector, which was then transfected into CHO cells using Attractene (QIAGEN). Electrophysiological studies were carried out 2 days after the transfection.

2.4. Electrophysiological measurements

APs and membrane currents were recorded from ventricular myocytes using ruptured and perforated whole-cell patch clamp methods. The composition of the pipette solutions and the bathing solutions are available in the on-line data supplement. All the experiments were carried out at 33–35 °C.

2.5. Quantitative RT-PCR analysis

Levels of mouse HCN1 (TaqMan assay ID: Mm00468832_m1), HCN2 (Mm00468538_m), HCN3 (Mm01212852_m1), HCN4 (Mm01176086_m1), Kir2.1 (Mm00434616_m1), Cav1.2 (Mm01188822_m1), Kv4.2 (Mm00807577_m1), Kchip2 (Mm00518915_g1) and Kv11.1 (Mm01161732_m1) mRNA were determined using quantitative real-time RT-PCR (qPCR) in predesigned TaqMan Gene Expression Assays (Applied Biosystems, Inc.). Relative levels of mRNA were normalized to the level of 18S rRNA.

2.6. ECG recording

Mice were anesthetized using 2.0% sevoflurane and placed in a supine position on a warming plate to maintain body temperature at around 37 °C. Two-lead ECGs (lead I, lead II) were recorded and analyzed using a PowerLab Data Acquisition System with LabChart software (AD Instruments Inc.). Vector ECGs were reconstructed using lead I and lead aVF. Lead aVF was calculated using following equation:

$$\text{lead aVF} = \frac{1}{\sqrt{3}} \times (2 \times \text{lead II} - \text{lead I})$$

2.7. Fluorescence immunohistochemistry

Mice were anesthetized with 3% sevoflurane and perfused through the left ventricle with heparinized saline followed by 4% paraformaldehyde in PBS. The hearts were removed and post-fixed for 2 h with 4% paraformaldehyde, cryoprotected for 18 h in 30% sucrose, and mounted in OCT Embedding Compound (Sakura Finetek, Japan), after

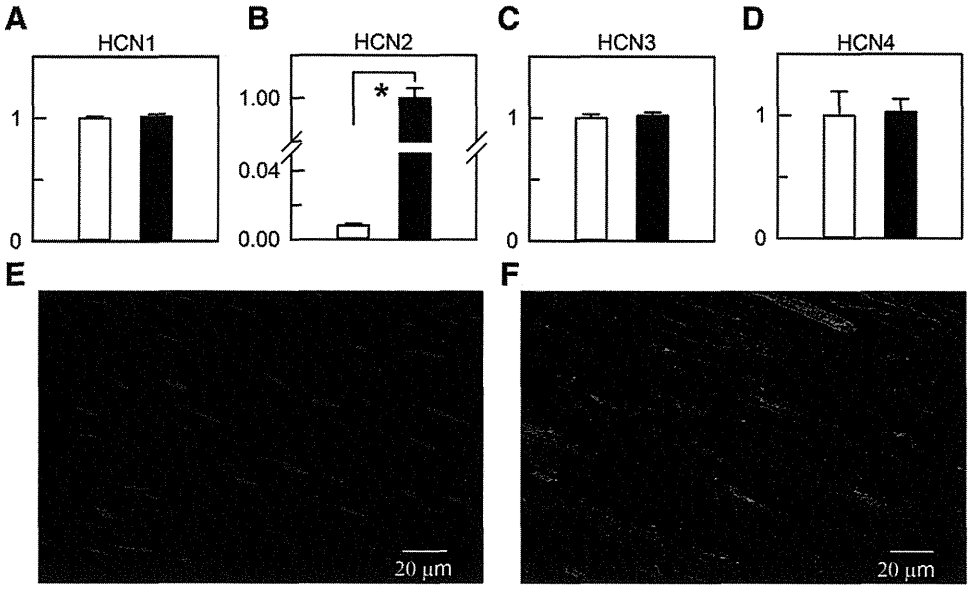

Fig. 1. Expression levels of HCN subtypes in the ventricles of HCN2-Tg mice (A–D) qPCR analysis of the relative mRNA level of HCN family proteins in ventricles from WT (white bars, $n = 5$) and HCN2-Tg (black bars, $n = 5$) mice. Note that the expression level of HCN2 mRNA is significantly higher in HCN2-Tg than WT hearts ($p < 0.01$). (E, F) Immunohistochemical staining for HCN2 demonstrating the subcellular localization of HCN2 in WT (E) and HCN2-Tg (F) ventricles. Nuclei were stained blue with DAPI. Bars represent 20 μm.

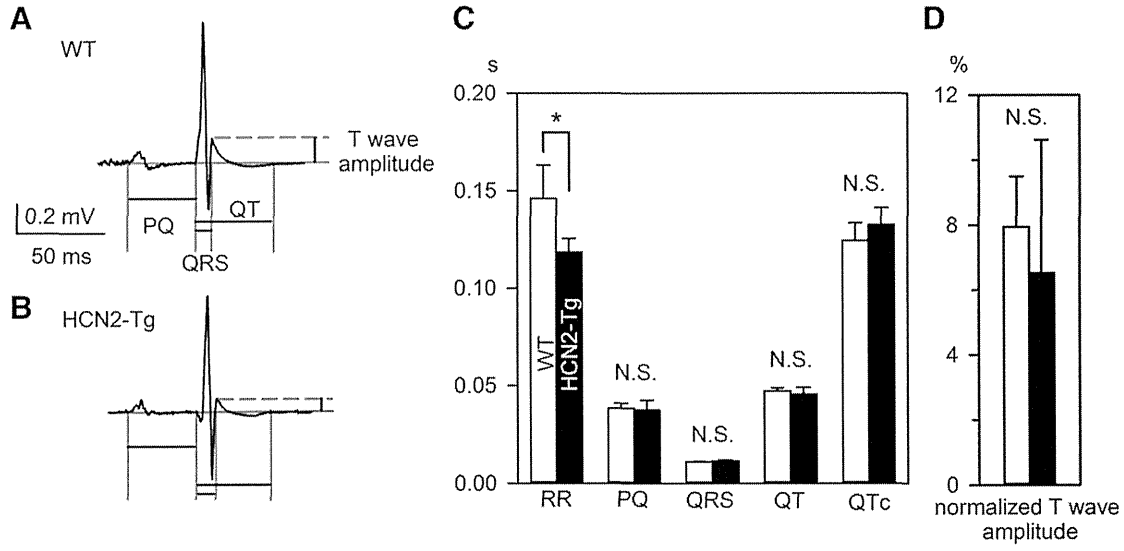

Fig. 2. ECG parameters in WT and HCN2-Tg mice (A, B) Representative ECG traces in WT (A) and HCN2-Tg (B) mice. Definitions of the PQ, QRS and QT intervals and the T-wave amplitude are indicated. (C) ECG parameters in WT (white bars, $n = 5$) and HCN2-Tg (black bars, $n = 5$) mice. In HCN2-Tg mice, RR intervals were significantly shorter than in WT mice. Other parameters (PR interval, QRS interval, QT interval, QTc (Bazett's Formula)) did not significantly differ between WT and HCN2-Tg mice. (D) Relative T-wave amplitudes in WT (white bar) and HCN2-Tg (black bar) mice.

which serial 5-μm sections were cut with a cryostat (CM3050S, Leica Microsystems, Wetzlar, Germany). The tissue sections were washed in PBS and then blocked with 5% normal goat serum (NGS) in PBS containing 0.05% Triton X-100. Thereafter, the sections were incubated with a polyclonal rabbit anti-HCN2 antibody (1:1000 dilution, Alomone Labs, Jerusalem, Israel) for 1 day at 4 °C, followed by incubation with Alexa Fluor 568 goat anti-rabbit IgG (1:2000 dilution, Invitrogen, Carlsbad, CA) for 2 h at room temperature. Images were captured using a Fluoview 1000 laser-scanning confocal microscope system (Olympus, Tokyo, Japan).

2.8. Statistical analysis

Data are shown as mean ± SD. Repeated-measures one-way analysis of variance (ANOVA) followed by the Tukey test and the Student's *t*-

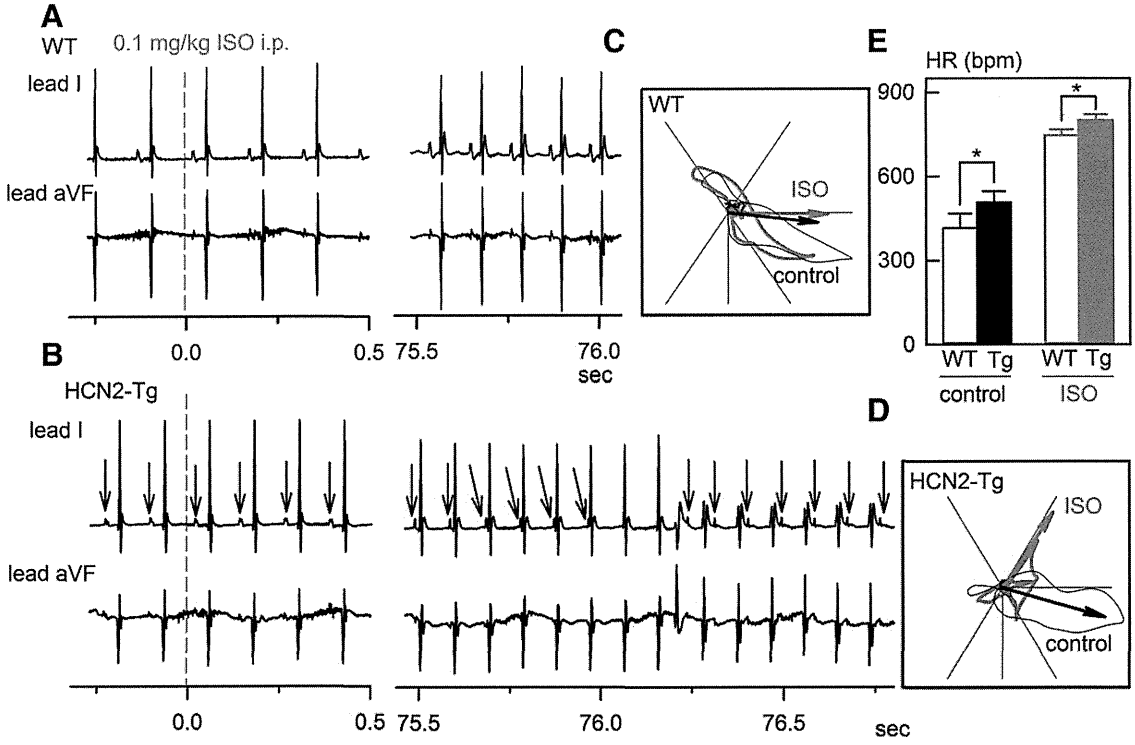

Fig. 3. Idioventricular rhythm induced by ISO in HCN2-Tg mice (A, B) Representative ECG traces in WT (A) and HCN2-Tg (B) mice. Under control conditions, we observed no arrhythmias in WT or HCN2-Tg mice. ISO (0.1 mg/kg) was intraperitoneally injected at 0 s. Note that in HCN2-Tg mice the ECG trace showed atrioventricular dissociation followed by idioventricular rhythm. The blue arrows indicate P waves to emphasize the AV dissociation. (C) Representative vector ECG in WT mice before (black) and after (red) ISO application. (D) Representative vector ECG in HCN2-Tg mice. ISO induced ectopic ventricular rhythm in HCN2-Tg hearts. (E) Heart rates in WT (open bar) and HCN2-Tg (filled bar) mice before (black) and after (red) ISO administration. With or without ISO, heart rates in HCN2-Tg mice were significantly faster than in WT mice.

test were used for data analysis. Differences were considered significant when $p < 0.05$.

3. Results

3.1. Isoproterenol (ISO) induces idioventricular rhythm in HCN2-Tg mice

Recent studies suggest that in addition to HCN2, HCN1 and HCN3 may also be involved in generating murine ventricular APs [13,14]. We therefore first examined whether the expression of these channels was altered in HCN2-Tg myocytes. qPCR experiments showed that there were no secondary changes in the expression of HCN1, HCN3 or HCN4 in HCN2-Tg myocytes. On the other hand, HCN2 expression was >100 times higher in HCN2-Tg than WT myocytes (Figs. 1A–D). Immunostaining confirmed that virtually no HCN2 was present in WT ventricular ventricles. In HCN2-Tg hearts, however, HCN2-immunoreactivity was ubiquitous throughout the ventricle (Fig. 1F).

Free moving, telemetric ECG records from HCN3 knockout mice ($HCN3^{-/-}$) revealed significant changes in the waveform: the QT interval was prolonged at lower heart rates in $HCN3^{-/-}$ mice, and the amplitude of the T-wave was greater [14]. By contrast, the only significant change in the ECG waveform in HCN2-Tg mice was a shortening of the RR interval (Fig. 2). The relative amplitude of the T-wave (normalized to the amplitude of the R-wave) varied considerably, and there was no significant difference between the WT ($7.9 \pm 1.5\%$, $n = 5$) and HCN2-Tg ($6.5 \pm 4.1\%$, $n = 5$, $p = 0.49$) hearts.

We previously reported that β-adrenergic stimulation increased the occurrence of ventricular arrhythmias during telemetric recording of ECGs in HCN2-Tg mice [10]. To explore the mechanism of this arrhythmia, we carried out electrocardiographic vector analysis under general anesthesia [15]. In WT mice, the intraperitoneal application of ISO (0.1 mg/kg) simply induced sinus tachycardia; no ventricular arrhythmias were observed, and the polarity of the QRS complex and the morphology of the vector loop were not significantly changed. By contrast, ISO-induced atrioventricular dissociation in HCN2-Tg mice, followed by idioventricular rhythm (Fig. 3B). These ventricular rhythms occurred intermittently and returned to sinus rhythm when the AV dissociation disappeared. Vector ECG revealed that upward vector loop and left

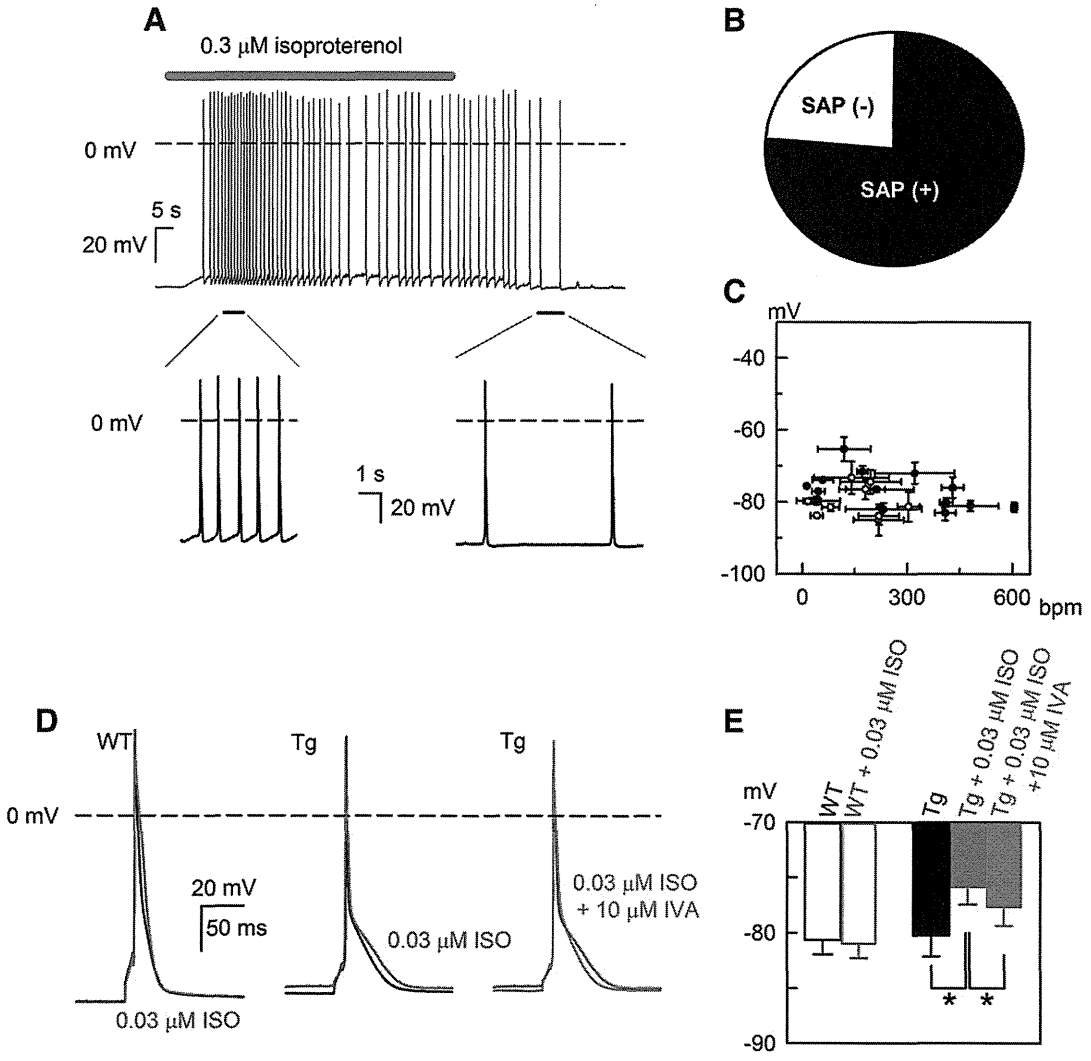

Fig. 4. ISO-induced SAP in HCN2-Tg myocytes (A) Continuous trace of a current-clamp recording from an HCN2-Tg myocyte. In this experiment, the membrane potential was recorded using the perforated patch method. The application of 0.3 μmol/L ISO is indicated by the red bar. (B) Fractions of ISO-treated HCN2-Tg myocytes with and without SAPs. The black sector indicates the percentage of myocytes exhibiting SAPs (76%). (C) Scatter plot of MDPs and firing rates (beats per min; bpm) of SAPs in ISO-treated HCN2-Tg myocytes: white symbols, data recorded using the perforated whole-cell patch method; black symbols, ruptured whole-cell patch method. Firing rates were calculated by successively averaging the inter-AP intervals in trains of SAPs; inter-AP intervals were measured from the onset of SAPs to the termination of ISO application. (D) Representative induced AP waveform in WT (left) and HCN2-Tg (center, right) myocytes. In HCN2-Tg, depolarization of RMP was observed at even lower concentration (0.03 μmol/L ISO). It should be noted that 10 μmol/L ivabradine significantly reversed the depolarization. In WT, ISO (red line) neither induced depolarization of RMP nor SAP. (E) RMPs in WT myocytes (open bars, $n = 6$) and in HCN2-Tg myocytes (filled bars, $n = 10$); control, black bars; with ISO, red bars; with ISO and IVA, green bar (repeated-measures one-way ANOVA followed by Tukey test, $^*p < 0.05$).

axis deviation were consistently induced during the idioventricular rhythm (Fig. 3D). These findings suggest that ISO increased ectopic pacemaker activity in the ventricles of HCN2-Tg hearts (Figs. 3A, C).

3.2. ISO induces depolarization and spontaneous APs in HCN2-Tg myocytes

To obtain insight into the cellular mechanism underlying the ectopic ventricular rhythm in HCN2-Tg mice, we recorded the membrane potentials of HCN2-Tg myocytes using pipette solution containing 5 mmol/L EGTA. As shown in Fig. 4A, the application of 0.3 μmol/L ISO depolarized the resting membrane potential (RMP) and often induced an irreversible train of spontaneous APs (SAPs); i.e., SAPs were observed in 76% of cells tested (32 of 42 cells, Fig. 4B). Fig. 4C summarizes the relationship between the average firing rates and the maximal diastolic potentials (MDPs) of SAPs in HCN2-Tg myocytes. The white symbols depict the values recorded in the perforated whole-cell patch experiments ($n = 9$), while the black symbols represent those recorded in the ruptured whole-cell patch experiments. However, the occurrence of SAPs did not differ between the experimental configurations. Twenty-four percent of ventricular myocytes isolated from HCN2-Tg hearts, ISO depolarized the RMP, but did not induced SAPs (data not shown). It was recently reported that HCN2 channel possessed permeability to Ca^{2+}, as well as Na^+ and K^+, which may induce delayed after depolarization (DAD) [16]. To test this possibility, we carried out fast pacing of HCN2-Tg myocytes. As shown in Supplementary Fig. 1, DAD was not induced both in the presence and absence of ISO, when recorded with 5 mmol/L EGTA pipette solution. These findings suggested that intracellular Ca^{2+}-dependent mechanism may not be involved in this automaticity.

In HCN2-Tg myocytes, ISO depolarized RMP even at lower concentration; 0.03 μmol/L ISO depolarized RMP from -80.2 ± 1.9 mV to -75.9 ± 1.6 mV (Fig. 4E, $n = 10$, $p < 0.05$). The depolarization of RMP was significantly reversed by the application of HCN channel blocker, ivabradine from -75.9 ± 1.6 mV to -77.6 ± 1.7 mV (Fig. 4E, $n = 10$, $p < 0.05$). In WT myocytes, ISO neither induced SAPs (data not shown) nor depolarized the RMP (Fig. 4D, left panel), which were -80.6 ± 1.3 mV and -81.0 ± 1.3 mV in the absence and presence of 0.03 μmol/L ISO, respectively (Fig. 4E, $n = 6$). ISO (0.3 μmol/L) also failed to induce SAP or depolarization in WT myocytes (data not shown).

To clarify the mechanisms underlying ISO-induced depolarization and SAPs, we next evaluated the membrane currents that contribute to the RMP. As shown in the right panel of Fig. 5A, inhibition of I_{K1} using 1 mmol/L Ba^{2+} unmasked a time-dependent inward current activated by hyperpolarizing pulses (i.e., I_h) in HCN2-Tg myocytes. In WT cells, I_h was negligibly small or absent when the K^+ concentration in the bathing solution was within the physiological range (Fig. 5A, left panel). The current–voltage (I–V) relationships for I_h (open circles) and the background current (filled circles) are shown in Fig. 5D.

We also compared the amplitudes of the inward-rectifier K^+ current (I_{K1}) measured as a Ba^{2+}-sensitive component. The I–V relationships in Fig. 5B show that I_{K1} density did not significantly differ between WT (open triangles) and HCN2-Tg (filled triangles) myocytes. Consistent with this observation, qPCR revealed that levels of Kir2.1 mRNA also did not significantly differ between WT and HCN2-Tg myocytes (Fig. 5C).

To determine whether I_h could be activated at membrane potentials close to the MDP or depolarized RMP in HCN2-Tg myocytes, we analyzed voltage-dependent, steady-state I_h activation curves before and after the application of ISO (Fig. 5E). We used a 2-step pulse protocol, in which conditioning pulses (to -50 and to -150 mV for 1250 ms) were followed by a test pulse to -150 mV, as shown in the upper panel of Fig. 5A. The amplitudes of the time-dependent components at the onset of test pulse were normalized as %activation and plotted. We then fitted the Boltzmann equation to each data set: %activation $= 1/(1 + \exp((V_m - V_{1/2})/s))$, where $V_{1/2}$ is the membrane potential at which activation is half-maximal, V_m is the membrane potential, and s is the slope factor. It is clear from Fig. 5E that $V_{1/2}$ was shifted from -118.5 ± 2.9 mV to -90.2 ± 1.5 mV by ISO application ($n = 4$, $p < 0.01$). These activation curves suggest that under control conditions 7% of I_h is activated at RMP, whereas in the presence of ISO as much as 25% of I_h is activated at the MDP (-77.1 ± 4.7 mV) of SAPs.

Finally, we compared the time course of the diastolic depolarization of SAPs and the activation time course of I_h in HCN2-Tg myocytes (Fig. 5F). As indicated by the dashed lines, the activation kinetics of I_h at -80 mV were so fast that the current could be sufficiently activated

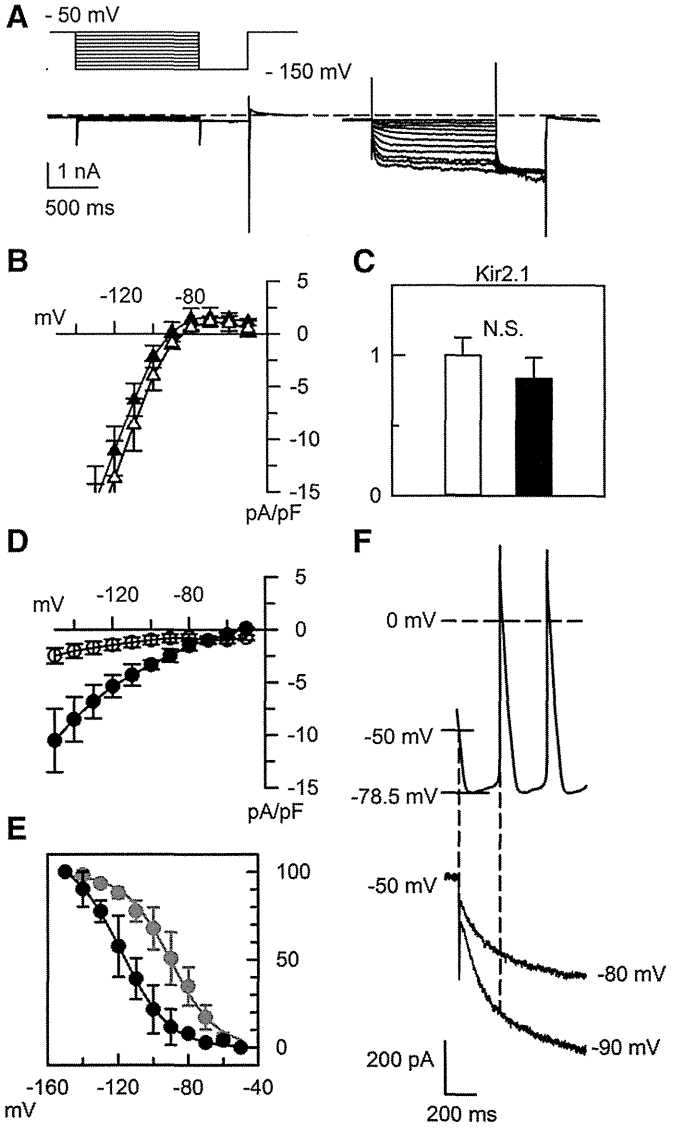

Fig. 5. Shift of the I_h activation curve underlies the depolarization of RMP in HCN2-Tg myocytes. (A) Representative current traces recorded from WT (left) and HCN2-Tg (right) myocytes after the application of 1 mmol/L Ba^{2+}. A robust I_h was revealed after complete inhibition of I_{K1}. The pulse protocol is indicated above the traces. (B) I–V relationship for I_{K1} in WT (open triangles) and HCN2-Tg (filled triangles) myocytes. I_{K1} amplitude was measured as the Ba^{2+}-sensitive component. (C) qPCR analysis of the relative levels of Kir2.1 mRNA in WT (open bar) and HCN2-Tg (filled bar) hearts ($n = 5$ in each group). (D) I–V relationship for I_h in HCN2-Tg myocytes (filled circles) in the presence of 0.3 μmol/L ISO. The amplitude of the time-dependent component during the conditioning pulse was measured as I_h and normalized to the cellular membrane capacitance. In WT myocytes, only the time-independent background current was observed (open circles). (E) Voltage-dependent steady-state activation curve for I_h in the presence (red circles) and absence (black circles) of 0.3 μmol/L ISO. (F) Upper panel shows an expanded SAP trace. The MDP was -78.5 mV, and the peak-to-peak interval was 209 ms. The lower panel shows the time course of I_h activation in HCN2-Tg myocytes at -80 and -90 mV. The membrane current was recorded in bathing solution containing 1 mmol/L Ba^{2+} and 0.3 μmol/L ISO.

at MDP during the beat-to-beat intervals between SAPs. This strongly suggests that in HCN2-Tg myocytes, ISO-induced depolarization of RMP and diastolic depolarization of SAPs are due to ISO-induced activation of HCN2.

3.3. Repolarization reserve in HCN2-Tg myocytes

Fenske et al. [14] recently reported detecting faint expression of HCN3 in ventricular myocytes from adult mice. They also reported that in HCN3 knockout ($HCN3^{-/-}$) mice, AP duration (APD) was shortened along with alteration of T-wave amplitude on ECGs. We therefore used ruptured whole-cell patch methods to evaluate the shape of APs induced in HCN2-Tg myocytes.

In Fig. 6A, AP was recorded in the absence of ISO. The black and red lines indicate APs of WT and HCN2-Tg, respectively. As summarized in Fig. 6C, the amplitude of action potential (APA) was not significantly different between HCN2-Tg and WT myocytes. AP duration at 90% repolarization (APD_{90}) was significantly longer, whereas APD_{50} and APD_{20} were significantly shorter in HCN2-Tg myocytes. Fig. 6B depicts the AP waveforms recorded in the presence of 0.3 μmol/L ISO. APs were induced in the same cells as in Fig. 6A. In HCN2-Tg myocyte, the RMP was depolarized due to the activation of HCN2. At the same time, and the amplitude of overshoot was reduced, most probably due to the inactivation of voltage-gated Na^+ current at depolarized RMP. Action potential parameters are summarized in Fig. 6C; APA was significantly smaller in HCN2-Tg. The differences of APD_{90}, APD_{50}, and APD_{20} were even more apparent in the presence of ISO.

At the given composition of the intra- and extracellular solutions, predicted reversal potential of I_h was −35 mV. During repolarization phase, it is therefore anticipated that outward tail current of I_h shortened APD at the membrane potentials more positive than −35 mV, and inward tail current of I_h prolonged APD at the membrane potentials more negative than −35 mV. To test this idea, we carried out AP clamp experiments in CHO cells expressing mouse HCN2 cDNA. We used CHO cells because they do not express voltage-gated K^+ currents, and it was easy to isolate I_h tail currents from the background current. We first activated I_h using a square pulse protocol with high-K^+ pipette solution containing 1 mmol/L cAMP (Fig. 7A). It should be noted that the direction of the tail current reversed between −40 and −30 mV. When we then perfused 5.4 mmol/L K^+, 10 mmol/L Cs^+ bathing solutions, inward I_h was almost completely blocked, but the outward tail current was less sensitive to this solutions.

In the same cell, we activated I_h using a command pulse shaped like an AP sampled from an HCN2-Tg myocyte in the presence of ISO (Fig. 7B, inset). In the left panel of Fig. 7B, the black line was recorded in the control bathing solution, the green line in the 5.4 mmol/L K^+, 10 mmol/L Cs^+ bathing solution. It is clear that a Cs^+-sensitive component was recorded during all phases of the AP. In the right panel of Fig. 7B, the *I–V* relationship was obtained from the repolarization phase in the AP clamp experiment ($n = 6$). The intersections between black line and magenta line show that the reversal potential of the Cs^+-sensitive component was close to −35 mV. It is evident from these results that the I_h tail current could participate in the repolarization phase of the mouse ventricular AP.

Finally, we confirmed that the expression of ion channels that could potentially affect APD was unchanged in HCN2-Tg myocytes. qPCR analyses showed that the expression of Cav1.2, Kv11.1, Kv4.2 and Kchip2 did not significantly differ between WT and HCN2-Tg myocytes. Furthermore, we detected no secondary changes in the densities of L-type Ca^{2+} currents and 4-AP-sensitive transient outward currents in HCN2-Tg myocytes (Supplementary Fig. 2).

4. Discussion

Evidence from numerous studies is suggestive of the potential arrhythmogenicity of HCNs in failing hearts but much remains unclear. For example, HCN2 and HCN4 are up-regulated in hypertrophied rat hearts and in the human failing heart [8,17,18]. In the mouse transverse aortic constriction (TAC) model, however, the amplitude of I_h is significantly increased, but there is a concomitant up-regulation of only HCN1

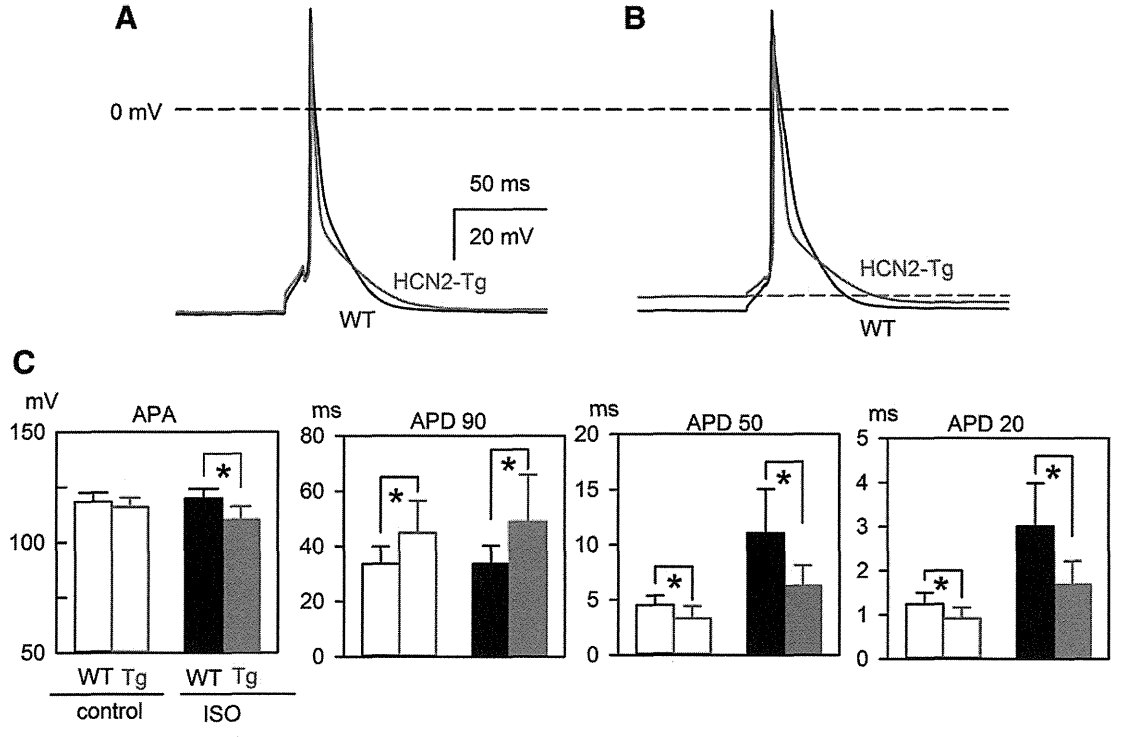

Fig. 6. Action potential parameters of induced APs (A) Representative AP traces of WT (black line) and HCN2-Tg myocyte (red line) under control condition. (B) AP traces in the presence of 0.3 μmol/L ISO. Black and red lines, same as in (A). As emphasized by the red dash line, depolarization of RMP was observed only in HCN2-Tg myocytes. (C) Summaries of APA, APD_{90}, APD_{50}, APD_{20}: black bars, WT; red bars, HCN2-Tg; open bars, without ISO; filled bars, with 0.3 μmol/L ISO. Bars depict means ± S.D., $^*p < 0.05$.

expression; expression of HCN2 and HCN4 is unaffected [13]. Moreover, none of the animal models of cardiac hypertrophy develop lethal arrhythmias. On the other hand, transgenic mice overexpressing a dominant-negative neuron-restricted silencing factor mutant (dnNRSF-Tg) die from ventricular tachyarrhythmia [9]. In the dnNRSF-Tg ventricle, robust increases in the expression of fetal cardiac channels, including HCN2 and HCN4 as well as CACNA1G and CACNA1H, two T-type Ca^{2+} channel subunits, have been reported [9], and blockade of HCN channels using ivabradine was recently shown to improve survival among dnNRSF-Tg mice [10]. This result is consistent with the potential arrhythmogenicity of HCN channels. It appears, however, that the overexpression of CACNA1G does not, by itself, provoke arrhythmias or SAPs in mouse ventricular myocytes; it only increases Ca^{2+} transients and induces mild cardiac hypertrophy [19]. Likewise, we showed that the overexpression of HCN2 is not, by itself, sufficient to induce lethal arrhythmia, but it induced an idioventricular rhythm under excessive β adrenergic stimulation. DADs are frequently observed in the myocytes isolated from hypertrophied heart. However, as shown in the present study, DADs were not induced by the overexpression of fetal type cardiac channels. These result suggested that the mechanism of ectopic automaticity in HCN2-Tg may be fundamentally different from that in hypertrophied heart.

In the present study, β-adrenergic stimulation consistently depolarized the RMP of HCN2-Tg myocytes. However, the magnitude of the depolarization did not directly correlate with the occurrence of SAPs, as depolarized RMPs in quiescent HCN2-Tg myocytes did not significantly differ from the MDPs of the SAPs. Why some cardiac myocytes (76%) exhibited SAPs while others (24%) did not remains unclear. In studies attempting to generate a "biological pacemaker" by overexpressing HCN2 in ventricular myocytes, the simultaneous overexpression of voltage-gated Na^+ channels (SkM1) was required for stable firing of SAPs [20]. This suggests, cell-to-cell variation in I_{Na} density may determine whether or not HCN2-Tg myocytes exhibit SAPs. In addition, I_{Na} and the T-type Ca^{2+} current ($I_{Ca\text{-}T}$) are activated at a similar range of membrane potentials [21]. Thus, the simultaneous overexpression of $I_{Ca\text{-}T}$ and I_h might induce stable SAPs in transgenic model mice and in hypertrophied hearts.

The firing rates of SAPs in HCN2-Tg myocytes were much less than 600 bpm. Because the heart rates of mice can easily increase to more than 700 bpm during β-adrenergic stimulation, the automaticity of HCN2-Tg ventricular myocytes may be masked by physiological pacing mediated via the cardiac conduction system [22,23]. Indeed, in this study ISO-induced ectopic ventricular rhythm in HCN2-Tg mice consistently preceded AV dissociation. Under physiological conditions, the pacemaker activity of the SA node might overdrive the idioventricular rhythm.

The repolarization phase of ventricular APs is primarily governed by activation of multiple K^+ currents, including I_{to}, the fast- and slow delayed rectifier K^+ currents (I_{Kr} and I_{Ks}; also known as HERG and KVLQT1), and I_{K1} [24–27]. This redundancy of repolarizing currents is called the "repolarization reserve" [28]. In the present study, we showed that when APs were recorded using the ruptured whole-cell patch method, the transgenic overexpression of HCN2 in mouse ventricular myocytes reduced the repolarization reserve and prolonged APD at the membrane potentials more negative than −35 mV. These results appear to be consistent with the observations reported in $HCN3^{-/-}$ myocytes, although the changes in APD were in the opposite direction in HCN2-Tg myocytes: in $HCN3^{-/-}$ myocytes, APD was shortened by

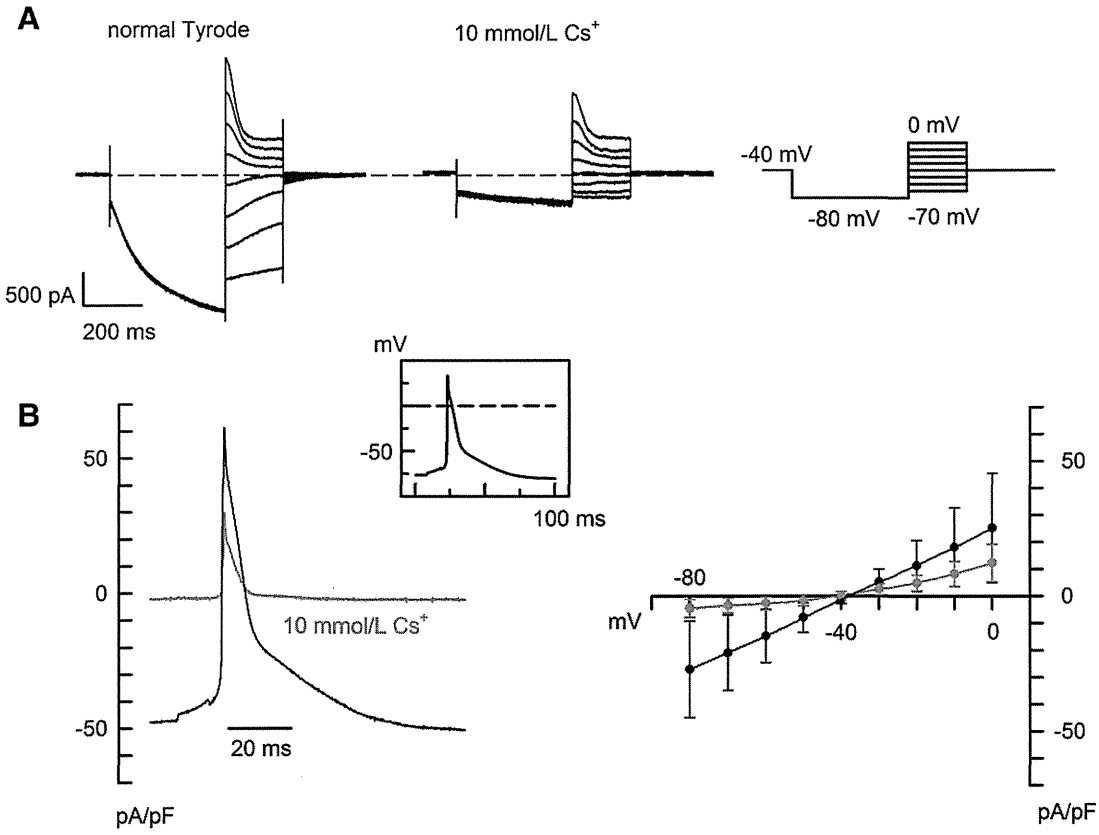

Fig. 7. Contribution of I_h tail currents to the repolarization phase of induced APs (A) HCN2 channels heterologously expressed in CHO cells were activated using a square pulse protocol (shown in the right panel). Family of I_h current before (left) and after (center) the application of 10 mmol/L Cs^+. The pipette solution contained 1 mmol/L cAMP. Note that the direction of the tail current reversed between −30 and −40 mV. (B) AP-shaped command pulses (inset) were applied to HCN2-expressing CHO cells at 0.5–5 Hz. The AP shape was sampled from HCN2-Tg myocytes in the presence of 0.3 μmol/L ISO. Left: the black trace depicts the membrane current recorded in control PBS; magenta, in 5.4 mmol/L K^+ 10 mmol/L Cs^+ bathing solution. Right: *I–V* relationship for the HCN2 current (black line) reconstructed from the repolarization phase of the AP clamp experiment in the left panel. The magenta line, recorded in 5.4 mmol/L K^+, 10 mmol/L Cs^+ bathing solution.

the reduction of inward I_h tail current at the membrane potentials more negative than −35 mV [14]. In our earlier report, this phenomenon may have been underestimated because we recorded the APs using the perforated patch method [10]. With that method, the Na^+-Ca^{2+} exchanger current driven by the intracellular Ca^{2+} transient reportedly affects the plateau phase of mouse ventricular APs at around −40 mV and might have masked the prolongation of APD in HCN2-Tg hearts [29]. It should be noted, however, that when the perforated patch method was used in mouse TAC experiments, ventricular I_h density was significantly increased and APD was significantly prolonged [13]. Reduction in repolarization reserve caused by I_h appears to be dependent on the time course of the I_h deactivation upon depolarization. Among the HCN subtypes, the order of the deactivation times at −60 mV was HCN3 > HCN4 > HCN1 > HCN2 [14]. In the present study, even HCN2, which possesses the fastest deactivation time, stayed open during the AP clamp experiments. In the hypertrophied hearts of larger animals, the expression of HCN2 and HCN4 is reportedly up-regulated [30]. Since HCN channels form heteromultimers, it would seem reasonable to expect that the time course of I_h deactivation in hypertrophied hearts would be intermediate, between those of HCN2 and HCN4, and would reduce the repolarization reserve in larger animals, whose cardiac myocytes exhibit longer APDs.

HCN channels reportedly possess Ca^{2+} permeability and re-expression of HCN channels may increase Ca^{2+} influx in hypertrophied heart [16]. The depolarization of RMP may also decrease driving force of Na^+/Ca^{2+} exchanger, thereby increasing intracellular Ca^{2+} concentration. Therefore, the pharmacological blockade of I_h may exert anti-arrhythmogenic effect by maintaining intracellular Ca^{2+} handling as well as repolarization reserve in hypertrophied heart [31].

5. Conclusions

Our findings demonstrate that the transgenic overexpression of HCN2 in the heart induces ectopic automaticity under β-adrenergic stimulation. The overexpression of HCN2 also reduces the repolarization reserve of the AP and prolongs APD. These results suggest that among fetal type cardiac channels re-expressed in heart failure, HCN2 alone is not sufficient to induce lethal arrhythmia, but it increases arrhythmogenic potential. Pharmacological blockade of HCN channels may therefore reduce the vulnerability of heart failure patients to ventricular arrhythmia.

5.1. Limitation of study

Plateau phase of mouse ventricular action potential is at ~−40 mV and is affected by intracellular Ca^{2+} transient. We therefore used Ca^{2+} buffering condition in order to evaluate the change of repolarization reserve in HCN2-Tg myocytes. On the other hand, HCN2 reportedly possesses Ca^{2+} permeability, which may potentially affect intracellular Ca^{2+} transient, giving rise to DADs and ventricular arrhythmia. This arrhythmogenic mechanism may be underestimated in the present study.

Disclosures

None declared.

Acknowledgments

We thank Ms. Hideko Yoshitake and Ms. Akemi Sakamoto for their secretarial work and Ms. Chiemi Sugiyama for her technical support.

This work was supported by a Grant-in-Aid for Scientific Research (B) from the Japan Society for the Promotion of Science (JSPS KAKENHI Grand Number 24300145) and a grant from the Ishibashi Foundation for the Promotion of Science.

Appendix A. Supplementary data

Supplementary data to this article can be found online at http://dx.doi.org/10.1016/j.yjmcc.2014.12.019.

References

[1] Wahl-Schott C, Biel M. HCN channels: structure, cellular regulation and physiological function. Cell Mol Life Sci 2009;66:470–94.
[2] Bucchi A, Baruscotti M, Robinson RB, DiFrancesco D. Modulation of rate by autonomic agonists in SAN cells involves changes in diastolic depolarization and the pacemaker current. J Mol Cell Cardiol 2007;43:39–48.
[3] Yasui K, Liu W, Opthof T, Kada K, Lee JK, Kamiya K, et al. I_f current and spontaneous activity in mouse embryonic ventricular myocytes. Circ Res 2001;88:536–42.
[4] Niwa N, Yasui K, Opthof T, Takemura H, Shimizu A, Horiba M, et al. $Ca_v3.2$ subunit underlies the functional T-type Ca^{2+} channel in murine hearts during the embryonic period. Am J Physiol Heart Circ Physiol 2004;286:H2257–63.
[5] Tomaselli GF, Beuckelmann DJ, Calkins HG, Berger RD, Kessler PD, Lawrence JH, et al. Sudden cardiac death in heart failure. The role of abnormal repolarization. Circulation 1994;90:2534–9.
[6] Nakayama H, Bodi I, Correll RN, Chen X, Lorenz J, Houser SR, et al. α1G-dependent T-type Ca^{2+} current antagonizes cardiac hypertrophy through a NOS3-dependent mechanism in mice. J Clin Invest 2009;119:3787–96.
[7] Wei-qing H, Qing-nuan K, Lin X, Cheng-hao G, Qi-yi Z. Expression of hyperpolarization-activated cyclic nucleotide-gated cation channel (HCN4) is increased in hypertrophic cardiomyopathy. Cardiovasc Pathol 2011;20:110–3.
[8] Fernández-Velasco M, Goren N, Benito G, Blanco-Rivero J, Boscá L, Delgado C. Regional distribution of hyperpolarization-activated current (I_f) and hyperpolarization-activated cyclic nucleotide-gated channel mRNA expression in ventricular cells from control and hypertrophied rat hearts. J Physiol 2003;553:395–405.
[9] Kuwahara K, Saito Y, Takano M, Arai Y, Yasuno S, Nakagawa Y, et al. NRSF regulates the fetal cardiac gene program and maintains normal cardiac structure and function. EMBO J 2003;22:6310–21.
[10] Kuwabara Y, Kuwahara K, Takano M, Kinoshita H, Arai Y, Yasuno S, et al. Increased expression of HCN channels in the ventricular myocardium contributes to enhanced arrhythmicity in mouse failing hearts. J Am Heart Assoc 2013;2:e000150-e.
[11] Oshita K, Igata S, Kuwabara Y, Kuwahara K, Ushijima K, Takano M. Isoproterenol-induced spontaneous action potentials in the cardiac myocytes of transgenic mouse overexpressing HCN2. J Physiol Sci 2013;63:S134.
[12] Takano M, Kinoshita H, Shioya T, Itoh M, Nakao K, Kuwahara K. Pathophysiological remodeling of mouse cardiac myocytes expressing dominant negative mutant of neuron restrictive silencing factor. Circ J 2010;74:2712–9.
[13] Hofmann F, Fabritz L, Stieber J, Schmitt J, Kirchhof P, Ludwig A, et al. Ventricular HCN channels decrease the repolarization reserve in the hypertrophic heart. Cardiovasc Res 2012;95:317–26.
[14] Fenske S, Mader R, Scharr A, Paparizos C, Cao-Ehlker X, Michalakis S, et al. HCN3 contributes to the ventricular action potential waveform in the murine heart. Circ Res 2011;109:1015–23.
[15] Kapoor N, Liang W, Marbán E, Cho HC. Direct conversion of quiescent cardiomyocytes to pacemaker cells by expression of Tbx18. Nat Biotechnol 2013;31:54–62.
[16] Yu X, Chen X-W, Zhou P, Yao L, Liu T, Zhang B, et al. Calcium influx through I_f channels in rat ventricular myocytes. Am J Physiol Cell Physiol 2007;292:1147–55.
[17] Stillitano F, Lonardo G, Zicha S, Varro A, Cerbai E, Mugelli A, et al. Molecular basis of funny current (I_f) in normal and failing human heart. J Mol Cell Cardiol 2008;45:289–99.
[18] Hoppe UC, Jansen E, Südkamp M, Beuckelmann DJ. Hyperpolarization-activated inward current in ventricular myocytes from normal and failing human hearts. Circulation 1998;97:55–65.
[19] Jaleel N, Nakayama H, Chen X, Kubo H, MacDonnell S, Zhang H, et al. Ca^{2+} influx through T- and L-type Ca^{2+} channels have different effects on myocyte contractility and induce unique cardiac phenotypes. Circ Res 2008;103:1109–19.
[20] Boink GJJ, Duan L, Nearing BD, Shlapakova IN, Sosunov EA, Anyukhovsky EP, et al. HCN2/SkM1 gene transfer into canine left bundle branch induces stable, autonomically responsive biological pacing at physiological heart rates. J Am Coll Cardiol 2013;61:1192–201.
[21] Kinoshita H, Kuwahara K, Takano M, Arai Y, Kuwabara Y, Yasuno S, et al. T-type Ca^{2+} channel blockade prevents sudden death in mice with heart failure. Circulation 2009;120:743–52.
[22] Galindo CL, Skinner MA, Errami M, Olson LD, Watson DA, Li J, et al. Transcriptional profile of isoproterenol-induced cardiomyopathy and comparison to exercise-induced cardiac hypertrophy and human cardiac failure. BMC Physiol 2009;9:23.
[23] Adachi T, Shibata S, Okamoto Y, Sato S, Fujisawa S, Ohba T, et al. The mechanism of increased postnatal heart rate and sinoatrial node pacemaker activity in mice. J Physiol Sci 2013;63:133–46.
[24] Nerbonne JM, Kass RS. Molecular physiology of cardiac repolarization. Physiol Rev 2005;85:1205–53.
[25] Ishihara K, Yan DH, Yamamoto S, Ehara T. Inward rectifier K^+ current under physiological cytoplasmic conditions in guinea-pig cardiac ventricular cells. J Physiol 2002;540:831–41.
[26] Babij P, Askew GR, Nieuwenhuijsen B, Su CM, Bridal TR, Jow B, et al. Inhibition of cardiac delayed rectifier K^+ current by overexpression of the long-QT syndrome HERG G628S mutation in transgenic mice. Circ Res 1998;83:668–78.

[27] Nattel S, Maguy A, Le Bouter S, Yeh YH. Arrhythmogenic ion-channel remodeling in the heart: heart failure, myocardial infarction, and atrial fibrillation. Physiol Rev 2007;87:425–56.
[28] Varró A, Baczkó I. Cardiac ventricular repolarization reserve: a principle for understanding drug-related proarrhythmic risk. Br J Pharmacol 2011;164:14–36.
[29] Wang J, Chan TO, Zhang XQ, Gao E, Song J, Koch WJ, et al. Induced overexpression of Na^+/Ca^{2+} exchanger transgene: altered myocyte contractility, $[Ca^{2+}]_i$ transients, SR Ca^{2+} contents, and action potential duration. Am J Physiol Heart Circ Physiol 2009; 297:H590–601.
[30] Herrmann S, Stieber J, Ludwig A. Pathophysiology of HCN channels. Pflugers Arch 2007;454:517–22.
[31] Swedberg K, Komajda M, Böhm M, Borer JS, Ford I, Dubost-Brama A, et al. Ivabradine and outcomes in chronic heart failure (SHIFT): a randomised placebo-controlled study. Lancet 2010;376:875–85.

Cardiovascular Research (2014) **104**, 183–193
doi:10.1093/cvr/cvu185

Inhibition of N-type Ca^{2+} channels ameliorates an imbalance in cardiac autonomic nerve activity and prevents lethal arrhythmias in mice with heart failure

Yuko Yamada[1,2†], Hideyuki Kinoshita[1,3†], Koichiro Kuwahara[1,3*], Yasuaki Nakagawa[1,3], Yoshihiro Kuwabara[1,4], Takeya Minami[1,3], Chinatsu Yamada[1,3], Junko Shibata[1,3], Kazuhiro Nakao[1,2,3], Kosai Cho[3,5], Yuji Arai[6], Shinji Yasuno[4], Toshio Nishikimi[1,3], Kenji Ueshima[4], Shiro Kamakura[7], Motohiro Nishida[8], Shigeki Kiyonaka[9], Yasuo Mori[9], Takeshi Kimura[3], Kenji Kangawa[2,10], and Kazuwa Nakao[1,11]

[1]Department of Medicine and Clinical Science, Kyoto University Graduate School of Medicine, 54 Shogoin Kawaharacho, Sakyo-ku, Kyoto 606-8507, Japan; [2]Department of Peptide Research, Kyoto University Graduate School of Medicine, Kyoto 606-8507, Japan; [3]Department of Cardiovascular Medicine, Kyoto University Graduate School of Medicine, Kyoto 606-8507, Japan; [4]Department of EBM Research, Institute for Advanced of Clinical and Translational Science, Kyoto University Hospital, Kyoto 606-8507, Japan; [5]Department of Primary Care and Emergency Medicine, Kyoto University Graduate School of Medicine, Kyoto 606-8507, Japan; [6]Department of Bioscience and Genetics, National Cerebral and Cardiovascular Center Research Institute, Suita 565-8565, Japan; [7]Department of Cardiovascular Medicine, National Cerebral and Cardiovascular Center, Suita 565-8565, Japan; [8]Division of Cardiocirculatory Signaling, Okazaki Institute for Integrative Bioscience (National Institute for Physiological Sciences), National Institute for Natural Sciences, Aichi 444-8787, Japan; [9]Department of Synthetic Chemistry and Biological Chemistry, Kyoto University Graduated School of Engineering, Kyoto 615-8530, Japan; [10]Department of Biochemistry, National Cerebral and Cardiovascular Center Research Institute, Suita 606-8507, Japan; and [11]Medical Innovation Center, Kyoto University Graduate School of Medicine, Kyoto 606-8507, Japan

Received 21 January 2014; revised 24 July 2014; accepted 30 July 2014; online publish-ahead-of-print 5 August 2014

Time for primary review: 10 days

Aims Dysregulation of autonomic nervous system activity can trigger ventricular arrhythmias and sudden death in patients with heart failure. N-type Ca^{2+} channels (NCCs) play an important role in sympathetic nervous system activation by regulating the calcium entry that triggers release of neurotransmitters from peripheral sympathetic nerve terminals. We have investigated the ability of NCC blockade to prevent lethal arrhythmias associated with heart failure.

Methods and results We compared the effects of cilnidipine, a dual N- and L-type Ca^{2+} channel blocker, with those of nitrendipine, a selective L-type Ca^{2+} channel blocker, in transgenic mice expressing a cardiac-specific, dominant-negative form of neuron-restrictive silencer factor (dnNRSF-Tg). In this mouse model of dilated cardiomyopathy leading to sudden arrhythmic death, cardiac structure and function did not significantly differ among the control, cilnidipine, and nitrendipine groups. However, cilnidipine dramatically reduced arrhythmias in dnNRSF-Tg mice, significantly improving their survival rate and correcting the imbalance between cardiac sympathetic and parasympathetic nervous system activity. A β-blocker, bisoprolol, showed similar effects in these mice. Genetic titration of NCCs, achieved by crossing dnNRSF-Tg mice with mice lacking *CACNA1B*, which encodes the α1 subunit of NCCs, improved the survival rate. With restoration of cardiac autonomic balance, dnNRSF-Tg:*CACNA1B*$^{+/-}$ mice showed fewer malignant arrhythmias than dnNRSF-Tg;*CACNA1B*$^{+/+}$ mice.

Conclusions Both pharmacological blockade of NCCs and their genetic titration improved cardiac autonomic balance and prevented lethal arrhythmias in a mouse model of dilated cardiomyopathy and sudden arrhythmic death. Our findings suggest that NCC blockade is a potentially useful approach to preventing sudden death in patients with heart failure.

Keywords Ion channel • Nervous system • Autonomic • Heart failure • Arrhythmia • N-type Ca^{2+} channel

* Corresponding author. Tel: +81 75 751 4287; fax: +81 75 771 9452. E-mail: kuwa@kuhp.kyoto-u.ac.jp

† These authors contributed equally to this work.

1. Introduction

Approximately 50% of deaths among patients with heart failure are classified as sudden death, mainly caused by lethal arrhythmias.[1] Despite recent progress, pharmacological interventions for the treatment and prevention of lethal arrhythmias associated with chronic heart failure remain unsatisfactory. Nonetheless, it is anticipated that a better understanding of the molecular basis of arrhythmicity in failing hearts will enable identification of therapeutic targets that can serve as the basis for the development of new pharmacological treatments.

Autonomic dysregulation leading to increased sympathetic nerve activity and decreased parasympathetic nerve activity contributes to the increased arrhythmicity seen in patients with chronic heart failure.[2,3] N-type voltage-dependent Ca^{2+} channels (NCCs), encoded by the *CACNA1B* (α1B subunit) gene, are predominantly localized in the nervous system, where they play a pivotal role in modulating a variety of neuronal functions, including neurotransmitter release at sympathetic nerve terminals.[4–6] Mice lacking *CACNA1B* show functional deterioration of their sympathetic nervous system,[7] and the ability of NCC blockade to prevent malignant arrhythmias and sudden death associated with heart failure remains unevaluated.

We previously reported that transgenic mice cardiac-selectively expressing a dominant-negative form of neuron-restrictive silencer factor (NRSF, also called REST) (dnNRSF-Tg), a transcriptional repressor important for regulation of the fetal cardiac gene program, showed progressive cardiomyopathy and sudden arrhythmic death beginning at about 8 weeks of age.[8] We have also reported several abnormalities in cardiac electrophysiological properties and ion channel expression in these dnNRSF-Tg mice.[9,10] The dnNRSF-Tg hearts showed increased expression of fetal-type ion channel genes, including *CACNA1H*, which encodes the T-type Ca^{2+} channel (TCC) α1 subunit, and a corresponding increase in $I_{ca,T}$ amplitude.[8] In that earlier study, we demonstrated that TCC blockade could prevent sudden death in dnNRSF-Tg mice by both restoring the normal electrophysiology of ventricular myocytes and correcting the cardiac autonomic dysfunction observed in dnNRSF-Tg mice.[11] Because TCC expression, and thus functional TCC currents, is increased in the myocardium of dnNRSF-Tg mice, TCC blockade directly affects the electrophysiological properties of ventricular myocytes in dnNRSF-Tg mice. On the other hand, the impact of modulating autonomic nervous system balance on the incidence of lethal arrhythmias in dnNRSF-Tg mice remains unclear.

Pharmacological blockade or genetic deletion of NCCs reportedly alters autonomic activity in both human patients and animal models.[7,12,13] On the other hand, little or no NCC expression has been detected in the ventricular myocardium. Therefore, to evaluate the extent to which correcting the autonomic imbalance prevents the lethal arrhythmias associated with heart failure, we assessed the effects of pharmacological blockade of NCCs and their genetic titration on arrhythmicity and sudden death in dnNRSF-Tg mice. Our findings demonstrate the importance of an imbalance between sympathetic and parasympathetic nerve activities in the generation of lethal arrhythmias in failing hearts and suggest that restoring autonomic nervous system balance through NCC inhibition can be an effective approach to preventing sudden arrhythmic death associated with heart failure.

2. Methods

An expanded Methods section is available in Supplementary material online.

2.1 Animal experiments

The animal care and all experimental protocols were reviewed and approved by the Animal Research Committee at Kyoto University Graduate School of Medicine, and conformed to the US National Institute of Health Guide for the Care and Use of Laboratory Animals. Beginning at 8 weeks of age, dnNRSF-Tg mice were left untreated (control) or were treated for 24 weeks with cilnidipine (10 mg/kg/day po) or nitrendipine (10 mg/kg/day po). The drug dosages were chosen based on earlier reports and our preliminary studies.[14,15] Cilnidipine was supplied by Mochida Pharmaceutical Co., Ltd (Tokyo, Japan). Nitrendipine was purchased from Wako Pure Chemical Industries, Ltd (Osaka, Japan). Bisoprolol was supplied by Mitsubishi Tanabe Pharma Corporation (Osaka, Japan). Cilnidipine exerts a much more potent inhibitory effect on N-type Ca^{2+} currents than does nitrendipine, which has little effect on N-type Ca^{2+} currents, particularly under conditions in which L-type Ca^{2+} current inhibition is comparable between the two drugs.[16,17] We then selected the doses of both drugs that similarly and minimally affected blood pressure. In another experiment, dnNRSF-Tg mice were bred with *CACNA1B* heterozygous knockout mice to obtain dnNRSF-Tg; $CACNA1B^{+/-}$ mice and control dnNRSF-Tg;$CACNA1B^{+/+}$ littermates. $CACNA1B^{+/-}$ mice were described in an earlier report.[7] For the isolation and analysis of hearts, mice were anaesthetized with 3.0% of isoflurane and sacrificed by cervical dislocation.

2.2 Statistical analysis

Data are presented as means ± standard errors of the mean (SEM) unless indicated otherwise. Survival was analysed using the Kaplan–Meier method with the log-rank test. Comparisons among multiple groups were made using ANOVA with post hoc Fisher's tests, except for numbers of arrhythmias. Values of $P < 0.05$ were considered significant. Numbers of arrhythmias between two groups were analysed using the Mann–Whitney test. Values of $P < 0.05$ were considered significant. Numbers of arrhythmias among four groups were analysed using Kruskal–Wallis non-parametric ANOVA followed by the Bonferroni correction. Values of $P < 0.0083$ were considered significant in that analysis.

3. Results

3.1 The dual N- and L-type Ca^{2+} channel blocker cilnidipine improves survival among dnNRSF-Tg mice without affecting cardiac structure or function

We initially confirmed that there is little expression of *CACNA1B*, encoding the α1 subunit of NCCs, in either wild-type (WT) or dnNRSF-Tg hearts, which is in contrast to its obvious expression in brain (*Figure 1A*). On the other hand, we detected substantially greater ventricular expression of *CACNA1H*, encoding the α1 subunit of TCCs, and *CACNA1C*, encoding the α1 subunit of L-type Ca^{2+} channels (*Figure 1B*). Although ventricular expression of *CACNA1B* is increased in dnNRSF-Tg hearts, probably due to the presence of NRSF-binding element in the gene, the levels are still lower than those of *CACNA1H* in WT hearts, where no functional T-type Ca^{2+}currents are detected.[11,18] To evaluate the potential therapeutic effect of modulating autonomic nervous system activity through NCC blockade on the development of malignant arrhythmias and sudden death in dnNRSF-Tg mice, we administered subpressor doses of cilnidipine, a dual N- and L-type dihydropyridine Ca^{2+} channel blocker, or nitrendipine, a more L-type-selective dihydropyridine Ca^{2+} channel blocker, to dnNRSF-Tg mice for 24 weeks, beginning when they were 8 weeks of age. Under our experimental conditions, systolic blood pressures and heart rates did not differ among the control, cilnidipine, and nitrendipine groups

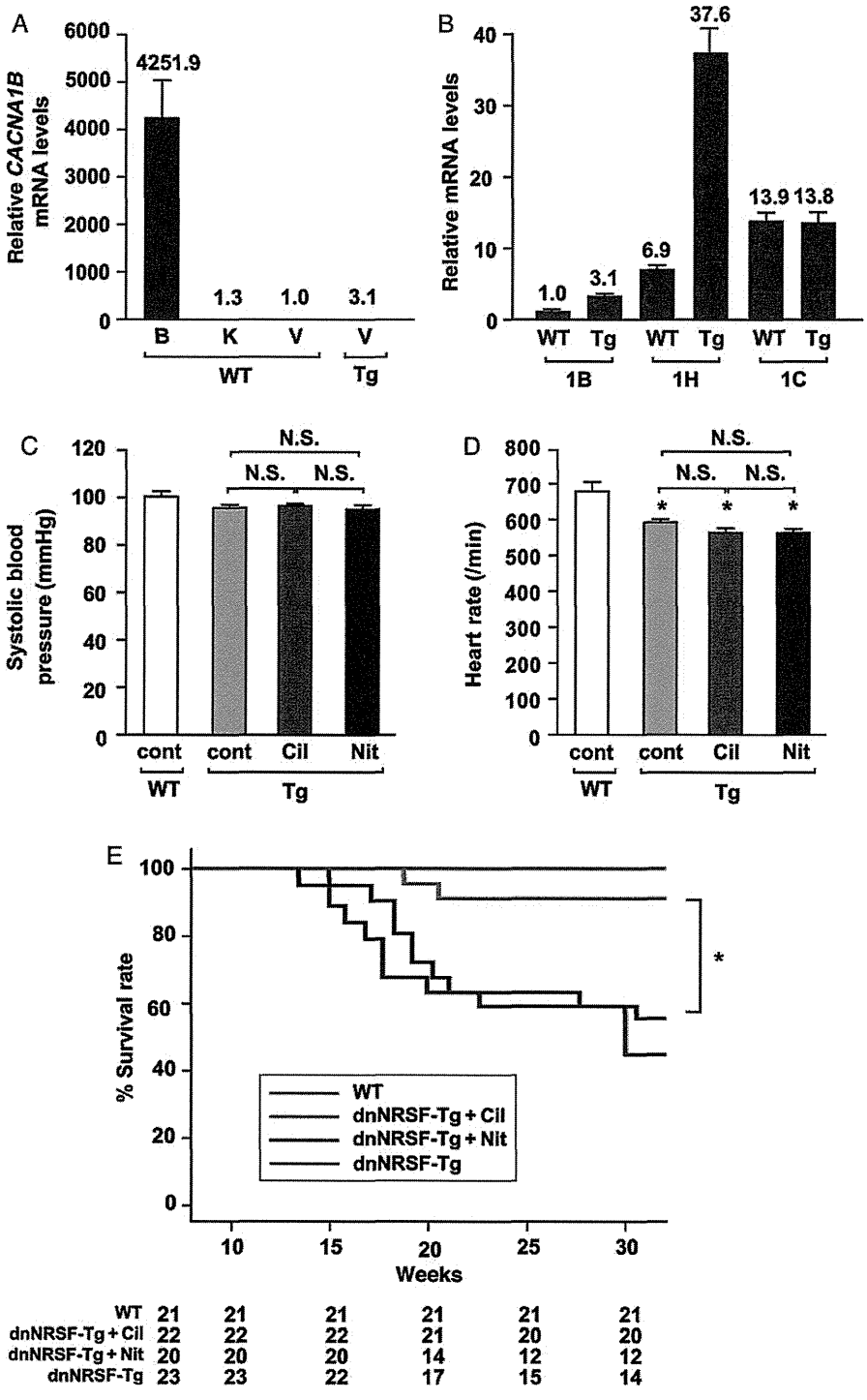

Figure 1 Pharmacological blockade of NCCs by cilnidipine improves survival among dnNRSF-Tg mice. (*A*) Relative levels of CACNA1B mRNA in brains (B) from WT, kidney (K) from WT, cardiac ventricle (V) from WT, and cardiac ventricle (V) from 8-week-old dnNRSF-Tg mice (Tg); levels in cardiac ventricle from WT mice were assigned a value of 1.0. $n = 3$ each for brain, kidney, and cardiac ventricle from WT mice and $n = 2$ for cardiac ventricle from dnNRSF-Tg mice. (*B*) Relative levels of CACNA1B, CACNA1H, and CACNA1C mRNA in cardiac ventricle from 8-week-old WT mice and dnNRSF-Tg mice (Tg); levels of CACNA1B mRNA in WT mice were assigned a value of 1.0. $n = 5$ for WT mice and $n = 7$ for dnNRSF-Tg. (*C* and *D*) Systolic blood pressures (*C*) and heart rates (*D*) in 20-week-old untreated WT, untreated Tg (Tg-cont), cilnidipine-treated Tg (Tg-Cil), and nitrendipine-treated Tg-Nit mice ($n = 15$ each for untreated Tg, Tg-Cil, and Tg-Nit, and $n = 10$ for untreated WT). ANOVA with post hoc Fisher's tests was used for analysis. *$P < 0.05$. N.S.: not significant. (*E*) Kaplan–Meyer survival curves for untreated WT, untreated Tg, Cil-treated Tg, and Nit-treated Tg over a 24-week drug administration period (from 8 to 32 weeks of age): Log-rank test was used for analysis. *$P < 0.05$ ($n = 21$ for WT, $n = 23$ for Tg without drugs, $n = 22$ for Tg + Cil, and $n = 20$ for Tg + Nit). The numbers of mice alive in each group at the end of each period are shown at the bottom of the figure. All data except survival curves are shown as means ± SEM.

of dnNRSF-Tg mice, though blood pressures were slightly lower and heart rates were significantly slower in dnNRSF-Tg mice than in untreated WT mice, as previously reported (systolic blood pressure: WT, 101.40 ± 1.48; Tg, 96.0 ± 1.75; Tg + cilnidipine, 96.67 ± 1.64; Tg + nitrendipine, 95.47 ± 1.92 mmHg and Heart rates: WT, 682.3 ± 27; dnNRSF-Tg, 590.6 ± 10.9; Tg + cilnidipine, 567.13 ± 17.58; Tg + nitrendipine, 568.8 ± 11.07/min) (*Figure 1C* and *D*).[8] We found that cilnidipine dramatically improved the survival rate among dnNRSF-Tg mice, compared with mice treated with nitrendipine or untreated control (*Figure 1E*). Although heart-to-body weight ratios were higher in dnNRSF-Tg than in WT mice, as reported previously,[8] heart-to-body weight ratios did not significantly differ among the control, cilnidipine, and nitrendipine groups of dnNRSF-Tg mice (WT, 4.08 ± 0.31; Tg, 5.94 ± 0.24; Tg + cilnidipine, 5.61 ± 0.48; Tg + nitrendipine, 5.94 ± 0.36 mg/g) (*Figure 2A*). Lung-to-body weight ratios also did not differ among these three groups (WT, 5.28 ± 0.37; Tg, 6.07 ± 0.22; Tg + cilnidipine, 5.93 ± 0.79; Tg + nitrendipine, 5.9 ± 0.29 mg/g) (*Figure 2B*). In addition, histological analyses, including determination of the %fibrotic area, and echocardiographic analyses also showed no significant differences among these three groups (*Figure 2C–F* and *Table 1*). In contrast, the echocardiography and histology showed that, compared with untreated WT mice, left ventricular systolic function was diminished and %fibrotic area was increased in dnNRSF-Tg mice, as reported previously (*Figure 2C–F* and *Table 1*).[8] Consistent with these findings, there was no significant difference in the expression of two cardiac stress marker genes, *ANP* and *SERCA2*, among the three groups, whereas their expression did differ between untreated WT mice and dnNRSF-Tg mice, as described previously (*Figure 2G* and *H*).[8]

Expression of the fibrosis-related genes *Col1a1*, *Col3a1*, and *FN1*, encoding collagen type1α1, collagen type3α1, and fibronectin 1, respectively, was not affected by the drug treatments (see Supplementary material online, *Figure S1A–C*). Expression of genes encoding the fetal-type ion channels *CACNA1H*, *HCN2*, and *HCN4* was higher in untreated dnNRSF-Tg ventricles than in control WT ventricles, as reported previously, and cilnidipine did not affect expression of these genes in dnNRSF-Tg ventricles (see Supplementary material online, *Figure S1D–F*). Collectively, all of these data indicate that cilnidipine suppresses sudden death in dnNRSF-Tg mice without significantly affecting cardiac structure or function.

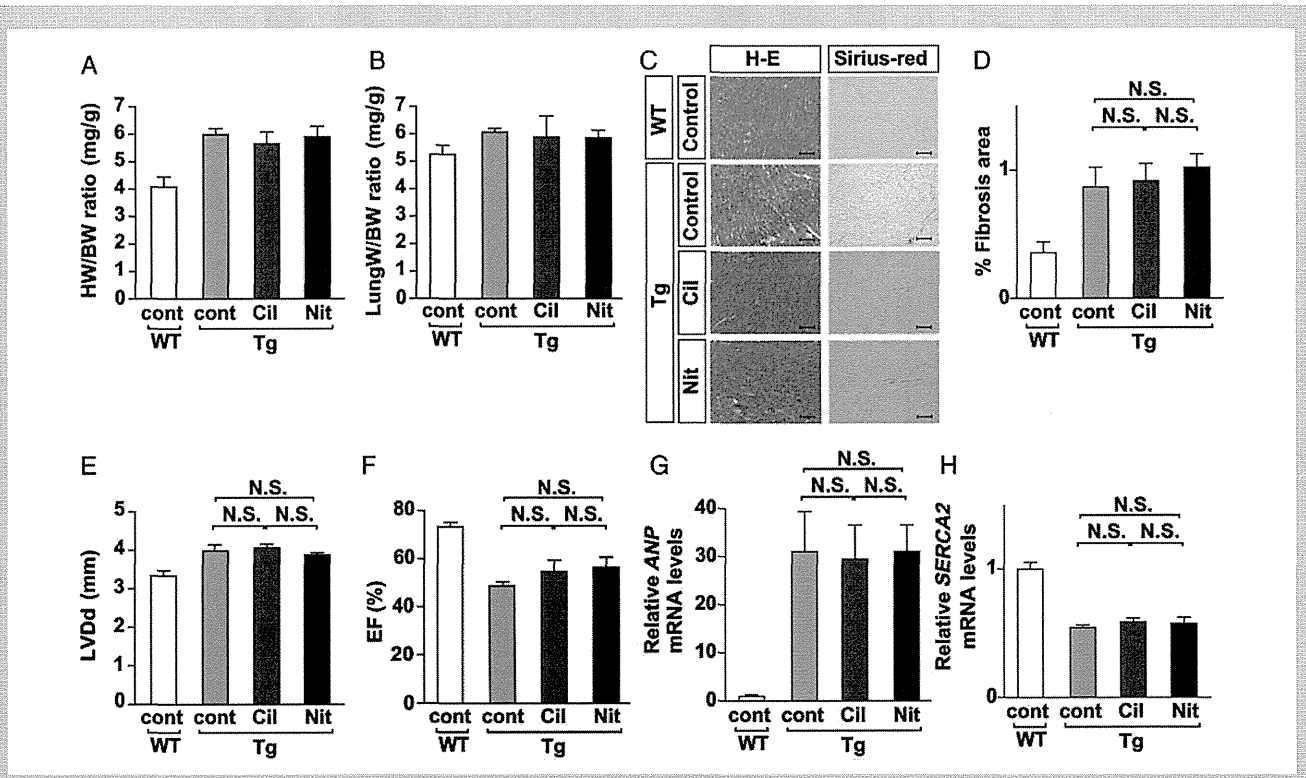

Figure 2 Cilnidipine does not affect cardiac structure or function in dnNRSF-Tg mice. (*A* and *B*) Heart-to-body weight (HW/BW) ratios (*A*) and lung-to-body weight (LungW/BW) ratios (*B*) in 20-week-old untreated WT (WT-cont), untreated Tg (Tg-cont), Cil-treated Tg (Tg-Cil), and Nit-treated Tg (Tg-Nit) mice ($n = 5$ for untreated WT, $n = 4$ for Tg-cont, $n = 4$ for Tg-Cil, and $n = 3$ for Tg-Nit). (*C*) Histology of hearts from 20-week-old untreated WT, Tg-cont, Tg-Cil, and Tg-Nit mice: H-E, haematoxylin-eosin staining; Sirius-red, Sirius-red staining. Scale bars = 100 μm. (*D*) %fibrotic area in 20-week-old untreated WT, Tg-cont, Tg-Cil, and Tg-Nit mice ($n = 5$ for Tg-cont; $n = 7$ for Tg-Cil). N.S.: not significant. (*E* and *F*) LVDd (*E*) and EF (*F*) assessed echocardiographically in untreated WT, Tg-cont, Tg-Cil, and Tg-Nit mice. *$P < 0.05$. N.S.: not significant. ($n = 5$ each for untreated WT, Tg-cont, and Tg-Cil; $n = 7$ for Tg-Nit). (*G* and *H*) Relative levels of ANP (*G*) and SERCA2 (*H*) mRNA in cardiac ventricles from untreated WT, Tg-cont, Tg-Cil, and Tg-Nit mice; levels in untreated WT were assigned a value of 1.0. N.S.: not significant. ($n = 4$ each). ANOVA with post hoc Fisher's tests was used for analysis. All data are shown as means ± SEM.

Table 1 Echocardiographic parameters in 20-week-old mice

	WT	dnNRSF-Tg		
	Control	Cont	Cil	Nit
Pharmacological inhibition				
LVDd (mm)	3.3 ± 0.13	3.9 ± 0.19	4.0 ± 0.11	3.8 ± 0.08
LVDs (mm)	2.1 ± 0.08	3.1 ± 0.17	3.1 ± 0.11	2.9 ± 0.10
IVST (mm)	0.76 ± 0.02	0.72 ± 0.02	0.72 ± 0.02	0.71 ± 0.03
PWT (mm)	0.76 ± 0.02	0.74 ± 0.02	0.76 ± 0.02	0.76 ± 0.03
FS (%)	36.1 ± 2.3	20.3 ± 1.4	23.3 ± 2.7	23.8 ± 2.4
EF (%)	73.2 ± 2.7	49.0 ± 2.3	55.4 ± 4.2	57.0 ± 4.3
			dnNRSF-Tg	
	$1B^{+/+}$	$1B^{+/-}$	$1B^{+/+}$	$1B^{+/-}$
Genetic titration				
LVDd (mm)	3.2 ± 0.10	3.3 ± 0.08	4.1 ± 0.12	3.3 ± 0.07*
LVDs (mm)	2.2 ± 0.12	2.2 ± 0.06	3.2 ± 0.13	2.3 ± 0.08*
IVST (mm)	0.66 ± 0.01	0.68 ± 0.02	0.66 ± 0.02	0.69 ± 0.02
PWT (mm)	0.68 ± 0.02	0.67 ± 0.02	0.66 ± 0.02	0.68 ± 0.02
FS (%)	31.8 ± 1.8	33.1 ± 1.9	20.4 ± 1.3	30.4 ± 1.3*
EF (%)	66.4 ± 2.4	68.9 ± 2.6	49.0 ± 2.4	64.3 ± 1.8*

Values are means ± SEM. Cil, cilnidipine; Nit, nitrendipine; $1B^{+/+}$, CACNA1B$^{+/+}$; $1B^{+/-}$, CACNA1B$^{+/-}$; LVDd, left ventricular diastolic dimension; LVDs, left ventricular systolic dimension; FS, fractional shortening; IVST, intraventricular septum wall thickness; PWT, posterior wall thickness. Numbers of mice tested in the pharmacological inhibition study are as follows: $n = 5$ for WT, untreated dnNRSF-Tg, and Cil-treated dnNRSF-Tg; $n = 7$ for Nit-treated dnNRSF-Tg (upper panel). Numbers of mice tested in the genetic titration study are as follows: $n = 13$ for $1B^{+/+}$, $n = 14$ for $1B^{+/-}$, $n = 11$ for dnNRSF-Tg;$1B^{+/+}$, and $n = 15$ for dnNRSF-Tg; $1B^{+/-}$ (lower panel). ANOVA with *post hoc* Fisher's tests was used for the analysis.
*$P < 0.05$ vs. dnNRSF-Tg;$1B^{+/+}$.

3.2 Cilnidipine improves cardiac autonomic nervous system function and reduces arrhythmicity in dnNRSF-Tg mice

We hypothesized that correcting autonomic balance through NCC blockade reduces arrhythmogenicity, thereby improving survival among dnNRSF-Tg mice. Heart rate variability (HRV) is a widely accepted index of cardiac autonomic nervous system activity.[19] Earlier frequency domain analysis of HRV revealed that patients with severe heart failure show a progressive reduction in power in both the low-frequency (LF) and high-frequency (HF) ranges,[19] and that a reduction in the LF power range is a significant predictor of sudden cardiac death in patients with heart failure.[20] We used HRV as an index to evaluate cardiac autonomic function in WT and dnNRSF-Tg mice, and examined the effects of cilnidipine on HRV.[19] In mice, HRV predominantly correlates with parasympathetic activity.[21] As we showed previously, both the LF and HF powers averaged over 24 h in dnNRSF-Tg mice (LF, 1.228 ± 0.198; HF, 0.823 ± 0.186 m/s^2) were markedly lower than in WT mice (LF, 4.331 ± 0.706; HF, 2.412 ± 0.089 m/s^2), indicating a general reduction in parasympathetic activity in dnNRSF-Tg mice (*Figure 3A* and *B*). Cilnidipine dramatically increased the power in both the LF and HF ranges of HRV (LF, 3.308 ± 0.338; HF, 2.228 ± 0.283 m/s^2), whereas nitrendipine had little effect on HRV (LF, 0.538 ± 0.447; HF, 1.383 ± 0.57 m/s^2) (*Figure 3A* and *B*). We also found that urinary excretion of norepinephrine, which is indicative of the level of sympathetic nerve activity, was significantly higher in dnNRSF-Tg than in WT mice, and that norepinephrine excretion was significantly reduced only by cilnidipine (WT, 0.09 ± 0.02; Tg, 0.33 ± 0.04; Tg + cilnidipine, 0.15 ± 0.03; Tg + nitrendipine, 0.32 ± 0.1 μg/day) (*Figure 3C*).

We next used an implanted telemetric monitoring system to examine the effects of cilnidipine and nitrendipine on electrocardiographic parameters in dnNRSF-Tg mice. We found that only cilnidipine significantly suppressed the number of premature ventricular contractions (PVCs) in dnNRSF-Tg hearts (WT, 0 ± 0; dnNRSF-Tg, 502.66 ± 305.69; dnNRSF-Tg + cilnidipine, 1.0 ± 0.66; dnNRSF-Tg + nitrendipine, 326.17 ± 147.24 /h) (*Figure 3D*). More importantly, it dramatically reduced the number of episodes of ventricular tachycardia (VT) (WT, 0 ± 0; dnNRSF-Tg, 14.92 ± 4.95; dnNRSF-Tg + cilnidipine, 0.06 ± 0.06; dnNRSF-Tg + nitrendipine, 12.75 ± 5.16/h) (*Figure 3E* and Supplementary material online, *Figure S2A* and *B*). These lines of evidence suggest that by restoring autonomic nervous system balance, cilnidipine reduces the incidence of lethal arrhythmias in dnNRSF-Tg mice.

3.3 β-Adrenergic receptor blockade prevents lethal arrhythmias and sudden death in dnNRSF-Tg mice

To verify the importance of correcting autonomic nervous system imbalance for the prevention of lethal arrhythmias and sudden death in dnNRSF-Tg mice, irrespective of effects on structural remodelling, we examined the effects of treating these mice with a β-adrenergic receptor blocker. We administered a subpressor dose of the lipophilic β-adrenergic receptor blocker bisoprolol (1 mg/kg/day po) to WT and dnNRSF-Tg mice. Although systolic blood pressures did not differ between untreated control and bisoprolol-treated mice (untreated WT, 107.5 ± 1.6; WT + bisoprolol, 108.0 ± 1.2; untreated Tg, 98.6 ± 2.0; Tg + bisoprolol, 98.6 ± 1.7 mmHg) (*Figure 3F*), heart rates were significantly slower in bisoprolol-treated than in untreated WT and dnNRSF-Tg mice (untreated WT, 697.8 ± 8.3; WT + bisoprolol,

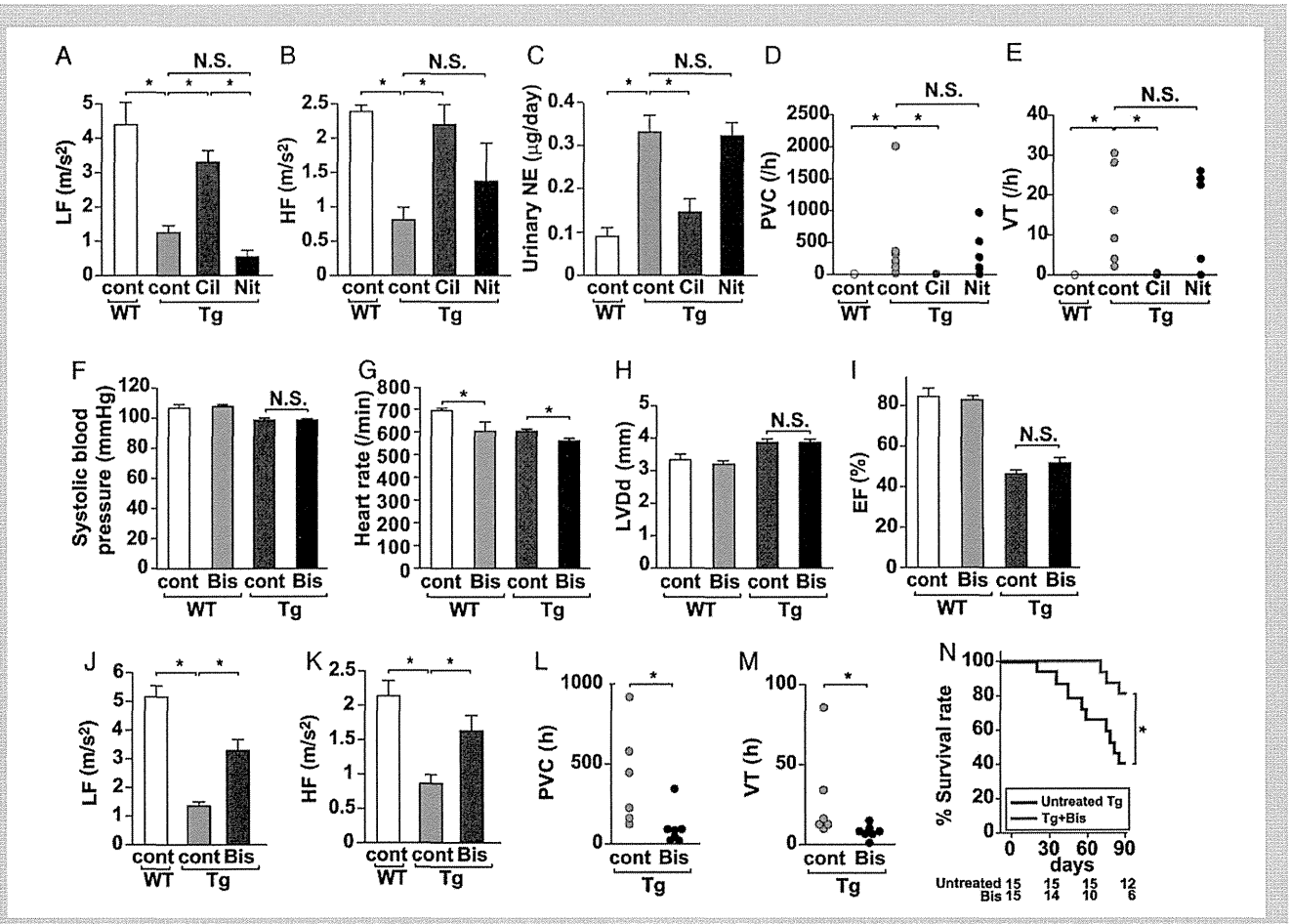

Figure 3 Cilnidipine restores cardiac autonomic nervous system balance and reduces arrhythmias in dnNRSF-Tg mice. (*A* and *B*) Average power of the LF (*A*) and HF (*B*) components of HRV recorded over a 24-h period in 20-week-old untreated WT (WT-cont), untreated Tg (Tg-cont), Cil-treated Tg (Tg-Cil), and Nit-treated (Tg-Nit) mice. $^*P < 0.05$. N.S.: not significant ($n = 5$ for WT, $n = 6$ for Tg-cont, $n = 8$ for Tg-Cil, and $n = 6$ for Tg-Nit). (*C*) Urinary norepinephrine (NE) levels in 20-week-old WT-cont, Tg-cont, Tg-Cil, and Tg-Nit mice. $^*P < 0.05$. N.S.: not significant ($n = 7$ for WT, $n = 7$ for Tg-cont, $n = 5$ for Tg-Cil, and $n = 4$ for Tg-Nit). (*D* and *E*) Numbers of PVC (*D*) and VT (*E*) recorded with a telemetry system in 20-week-old WT-cont, Tg-cont, Tg-Cil, and Tg-Nit mice are shown by dot plots. $^*P < 0.0083$, N.S.: not significant ($n = 5$ for WT-cont, $n = 6$ for Tg-cont, $n = 8$ for Tg-Cil, and $n = 6$ for Tg-Nit). (*F* and *G*) Systolic blood pressures (*F*) and heart rates (*G*) in 20-week-old untreated WT (WT-cont), bisoprolol (Bis)-treated WT (WT-Bis), untreated Tg (Tg-cont), and Bis-treated Tg (Tg-Bis) mice ($n = 4$ for WT-cont, $n = 3$ for WT-Bis, and $n = 5$ for Tg-cont and Tg-Bis). (*H* and *I*) LVDd (*H*) and EF (*I*) assessed echocardiographically in WT-cont, WT-Bis, Tg-cont, and Tg-Bis mice. $^*P < 0.05$. N.S.: not significant. ($n = 4$ for WT-cont, $n = 3$ for WT-Bis, and $n = 5$ for Tg-cont and Tg-Bis). (*J* and *K*) Average power of the LF (*J*) and HF (*K*) components of heart rate variability (HRV) recorded over a 24-h period in 20-week-old WT-cont, Tg-cont, and Tg-Bis mice. $^*P < 0.05$. N.S.: not significant ($n = 4$ for WT-cont, $n = 6$ for Tg-cont, and $n = 7$ for Tg-Bis). (*L* and *M*) Numbers of PVC (*L*) and VT (*M*) recorded with a telemetry system in 20-week-old Tg-cont and Tg-Bis mice are shown by dot plots. $^*P < 0.05$ ($n = 6$ for Tg-cont; $n = 7$ for Tg-Bis). ANOVA with post hoc Fisher's tests was used for analysis, except for numbers of arrhythmias (*D*, *E*, *L*, and *M*). Numbers of arrhythmias among the four groups were analyzed using Kruskal–Wallis non-parametric ANOVA followed by the Bonferroni correction (*D* and *E*). Numbers of arrhythmias between two groups were analyzed using non-parametric Mann–Whitney test (*L* and *M*). (*N*) Kaplan–Meyer survival curves for untreated Tg and Bis-treated Tg (Tg + Bis) over a 90-day drug administration period (from 12 to 25 weeks of age): Log-rank test was used for the survival analysis. $^*P < 0.05$ ($n = 15$ each). The numbers of mice alive in each group at the end of each period are shown at the bottom of the figure. All data except numbers of arrhythmias and survival curves are shown as means ± SEM.

604.7 ± 38.3; Tg, 601.6 ± 10.1; Tg + bisoprolol, 558.6 ± 12.0/min) (*Figure 3G*). At the dose tested, bisoprolol also did not affect cardiac systolic function assessed echocardiographically in dnNRSF-Tg mice [LVDd: WT, 3.3 ± 0.2; WT + bisoprolol, 3.2 ± 0.1; Tg, 3.9 ± 0.1; Tg + bisoprolol, 3.9 ± 0.1 mm and ejection fraction (EF): WT, 84.5 ± 4.0; WT + bisoprolol, 83.0 ± 1.5; Tg, 46.0 ± 1.6; Tg + bisoprolol, 51.5 ± 2.7%] (*Figure 3H* and *I*). On the other hand, bisoprolol significantly restored power in both the LF and HF ranges of HRV (LF: untreated WT, 5.19 ± 0.37; Tg, 1.36 ± 0.14; Tg + bisoprolol, 3.34 ± 0.39 m/s^2 and HF: untreated WT, 2.12 ± 0.24; Tg, 0.86 ± 0.12; Tg + bisoprolol, 1.62 ± 0.22 m/s^2) (*Figure 3J* and *K*) and reduced the incidence of PVCs and VTs in those mice (PVC: Tg, 408.3 ± 122.9; Tg + bisoprolol, 98.9 ± 42.2/h; VT: Tg, 28.2 ± 12.1; Tg + bisoprolol, 7.6 ± 1.7/h) (*Figure 3L* and *M*). As a result, bisoprolol significantly improved survival rates among dnNRSF-Tg mice (*Figure 3N*). These results strongly support our finding that imbalance of autonomic nervous system

activities is critically involved in the occurrence of sudden arrhythmic death in dnNRSF-Tg mice.

3.4 Genetic titration of NCC improves survival among dnNRSF-Tg mice

To further confirm the benefit of NCC inhibition for prevention of sudden death in dnNRSF-Tg mice, we next genetically titrated NCC expression by crossing dnNRSF-Tg mice with mice lacking *CACNA1B*, encoding the α1B subunit of NCC. Because the *CACNA1B*$^{-/-}$ genotype has a high incidence of early mortality from an as yet unknown cause, we compared the phenotypes of dnNRSF-Tg;*CACNA1B*$^{+/+}$ mice with those of dnNRSF-Tg;*CACNA1B*$^{+/-}$ mice, in which NCC expression is reduced to ~52.9% of that in dnNRSF-Tg;*CACNA1B*$^{+/+}$ mice (*Figure 4A*). The gross appearance of *CACNA1B*$^{+/-}$ mice is normal, and they show no early mortality. Systolic blood pressures in dnNRSF-Tg;*CACNA1B*$^{+/-}$ and dnNRSF-Tg;*CACNA1B*$^{+/+}$ mice did not significantly differ, but they were mildly lower than in control WT (*CACNA1B*$^{+/+}$) mice (WT, 101.25 ± 7.26; *CACNA1B*$^{+/-}$, 91.25 ± 2.78; dnNRSF-Tg, 92 ± 4.38; dnNRSF-Tg;*CACNA1B*$^{+/-}$, 89.25 ± 2.14 mmHg) (*Figure 4B*). Similarly, heart rates did not differ between dnNRSF-Tg;*CACNA1B*$^{+/+}$ and dnNRSF-Tg;*CACNA1B*$^{+/-}$ mice, although they were slower in dnNRSF-Tg;*CACNA1B*$^{+/+}$ than in control WT mice, as reported previously (WT, 632.25 ± 26.36; *CACNA1B*$^{+/-}$, 594 ± 33.39; dnNRSF-Tg, 515.25 ± 14.71; dnNRSF-Tg;*CACNA1B*$^{+/-}$, 521.5 ± 23.32/min) (*Figure 4C*).[8] Body weights were comparable between the two dnNRSF-Tg groups (WT, 31.08 ± 1.11; *CACNA1B*$^{+/-}$, 29.53 ± 1.37; dnNRSF-Tg; 28.86 ± 1.19; dnNRSF-Tg;*CACNA1B*$^{+/-}$, 27.41 ± 1.09 g) (*Figure 4D*), but heart-to-body weight ratios were higher in dnNRSF-Tg;*CACNA1B*$^{+/+}$ than in WT (*CACNA1B*$^{+/+}$) mice and were significantly lower in dnNRSF-Tg;*CACNA1B*$^{+/-}$ than in dnNRSF-Tg;*CACNA1B*$^{+/+}$ mice (WT, 4.44 ± 0.04; *CACNA1B*$^{+/-}$, 4.51 ± 0.14; dnNRSF-Tg; 5.68 ± 0.21; dnNRSF-Tg;*CACNA1B*$^{+/-}$, 4.86 ± 0.18 mg/g) (*Figure 4E*). Lung-to-body weight ratios were comparable between the two dnNRSF-Tg groups (WT, 5.06 ± 0.22; *CACNA1B*$^{+/-}$, 4.68 ± 0.96; dnNRSF-Tg; 5.41 ± 0.09; dnNRSF-Tg; *CACNA1B*$^{+/-}$, 5.52 ± 0.26 mg/g) (*Figure 4F*). Echocardiographic analysis showed that left ventricular diastolic dimension (LVDd) was higher in dnNRSF-Tg;*CACNA1B*$^{+/+}$ than in WT mice, whereas EF was lower in dnNRSF-Tg;*CACNA1B*$^{+/+}$ than in WT mice, as was reported previously (*Figure 5A* and *B*).[8] In addition, LVDd was lower and EF was higher in dnNRSF-Tg;*CACNA1B*$^{+/-}$ than in dnNRSF-Tg;*CACNA1B*$^{+/+}$ mice (*Figure 5A* and *B* and *Table 1*).

Histological analysis revealed no significant difference between dnNRSF-Tg;*CACNA1B*$^{+/+}$ and dnNRSF-Tg;*CACNA1B*$^{+/-}$ mice, although %fibrotic area showed a trend towards being smaller in dnNRSF-Tg;*CACNA1B*$^{+/-}$ than in dnNRSF-Tg;*CACNA1B*$^{+/+}$ mice (*Figure 5C* and *D*). Expression of the fibrosis-related genes *Col1a1*, *Col3a1*, and *FN1* did not significantly differ between dnNRSF-Tg;*CACNA1B*$^{+/+}$ and dnNRSF-Tg;*CACNA1B*$^{+/-}$ mice (see Supplementary material online, *Figure S3A–C*), though there was a significant difference in the expression of *ANP* and *SERCA2* between these two genotypes (*Figure 5E* and *F*). Genetic reduction in *CACNA1B* also significantly affected expression of *CACNA1H* and *HCN2*, but not *HCN4*, in dnNRSF-Tg ventricles (see Supplementary material online, *Figure S3D–F*). All of these data demonstrate that genetic reduction of *CACNA1B* tends to ameliorate impaired cardiac function and pathological remodelling in dnNRSF-Tg mice. Furthermore, survival among dnNRSF-Tg;*CACNA1B*$^{+/-}$ mice was dramatically and significantly better than among control dnNRSF-Tg;*CACNA1B*$^{+/+}$ mice (*Figure 6A*), demonstrating that reduction of NCC prevents sudden arrhythmic death in dnNRSF-Tg mice.

3.5 Reducing *CACNA1B* expression improves autonomic function and decreases the occurrence of arrhythmias in dnNRSF-Tg mice

We also assessed autonomic nervous system activity in dnNRSF-Tg;*CACNA1B*$^{+/-}$ and dnNRSF-Tg;*CACNA1B*$^{+/+}$ mice. In HRV analyses, the reductions in LF and HF power otherwise seen in dnNRSF-Tg;*CACNA1B*$^{+/+}$ mice (LF, 1.288 ± 0.16; HF, 1.168 ± 0.108 m/s^2) were significantly ameliorated in dnNRSF-Tg;*CACNA1B*$^{+/-}$ mice (LF, 3.54 ± 0.47; HF, 3.075 ± 0.468 m/s^2), indicating a restoration of parasympathetic activity through reduction of NCC function (*Figure 6B* and *C*). In addition, we found that the increase in urinary excretion of norepinephrine seen in dnNRSF-Tg;*CACNA1B*$^{+/+}$ mice (0.428 ± 0.07 μg/day) was significantly ameliorated in dnNRSF-Tg;*CACNA1B*$^{+/-}$ mice (0.154 ± 0.05 μg/day) (*Figure 6D*). Finally, evaluation of arrhythmicity revealed that the incidences of both PVCs and VT were significantly lower in dnNRSF-Tg;*CACNA1B*$^{+/-}$ than in dnNRSF-Tg;*CACNA1B*$^{+/+}$ mice (PVC: WT, 0 ± 0; *CACNA1B*$^{+/-}$, 0 ± 0; dnNRSF-Tg, 239.08 ± 27.93; dnNRSF-Tg;*CACNA1B*$^{+/-}$, 3.21 ± 3.21 and VT: WT, 0 ± 0; *CACNA1B*$^{+/-}$, 0 ± 0; dnNRSF-Tg, 41.3 ± 12.69; dnNRSF-Tg;*CACNA1B*$^{+/-}$, 0.36 ± 0.36/h) (*Figure 6E* and *F*). These results demonstrate that genetic titration of *CACNA1B*, encoding NCC, corrected an imbalance between sympathetic and parasympathetic nervous system activities, which, at least in part, contributes to reducing malignant arrhythmias in dnNRSF-Tg mice in a manner similar to pharmacological NCC blockade.

4. Discussion

Autonomic dysregulation leading to increased sympathetic nerve activity and reduced parasympathetic nerve activity is reportedly associated with the increased arrhythmicity seen in patients with chronic heart failure.[2,22,23] NCCs play a major role in the release of norepinephrine at sympathetic nerve terminals.[7,24] Consequently, mice lacking *CACNA1B*, the gene encoding the α1 subunit of NCCs, exhibit a significantly impaired positive inotropic response.[7] In the present study, we found that pharmacological blockade of NCCs or their genetic titration improved the balance between sympathetic and parasympathetic nerve activities and prevented the sudden death and arrhythmicity otherwise seen in dnNRSF-Tg mice, a mouse model of sudden arrhythmic death associated with cardiac dysfunction.[8] The mode of death in these model mice is sudden and without overt oedema, pleural effusion, or apparent lung congestion, and all the telemetry data obtained at the time of death indicate VT/VF to be the cause.[8] Moreover, in an earlier study, we found that systemic administration of isoproterenol induced VT more frequently in dnNRSF-Tg than in WT mice.[11] Conversely, administration of a β-blocker led to a significant reduction in the incidence of sudden death among dnNRSF-Tg mice under conditions in which cardiac systolic function and remodelling were not affected (*Figure 3H–N*). These findings suggest that NCC blockade or genetic titration of NCC reduces the likelihood of sudden arrhythmic death, thereby improving survival.

Pharmacological interventions that reduce cardiac sympathetic activity have been shown to protect against arrhythmias,[25] while